

Geochronology and Sr–Nd–Hf isotope constraints on the petrogenesis of teschenites from the type-locality in the Outer Western Carpathians

IRENA BRUNARSKA and ROBERT ANCZKIEWICZ[✉]

Institute of Geological Sciences, Polish Academy of Sciences, Kraków Research Centre, Senacka 1, 31-002 Kraków, Poland;
 ✉ndanczki@cyfronet.pl

(Manuscript received September 21, 2018; accepted in revised form May 9, 2019)

Abstract: The Teschenite Association Rocks (TAR) in the Outer Western Carpathian (OWC) flysch form a classic suite of alkaline intrusions where *teschenite* and *picrite* were first defined. They represent continental intraplate volcanism that produced a wide range of melano- to mesocratic rocks emplaced during the Early Cretaceous rifting within the southern margin of the European Plate. Geochemical modelling indicates that they may be a product of ~2–5 % partial melting of the metasomatised, asthenospheric mantle. The variations in REE (low/heavy REE content, $\text{La}_{\text{N}}/\text{Yb}_{\text{N}}=11\text{--}34$) are consistent with deep melting of garnet peridotite. Initial $\epsilon(\text{Nd})_i=5.0\text{--}6.3$ and $\epsilon(\text{Hf})_i=4.9\text{--}10.0$ preclude the significant mature crust involvement. Instead, a linear array formed by the $^{143}\text{Nd}/^{144}\text{Nd}$ and $^{176}\text{Hf}/^{177}\text{Hf}$ isotopic ratios points to a genesis from the mixed, HIMU–OIB source with the more depleted, MORB-type component. Mantle metasomatism was most likely caused by the Variscan subduction–collision processes as indicated by the depleted mantle Nd model ages. The isotope and trace element ratios of the TAR resemble the European Asthenospheric Reservoir (EAR) — the common mantle end-member for the widespread Cenozoic volcanic rocks in Europe. This confirms a long-term existence of the EAR mantle component beneath the Central Europe, at least since the Early Cretaceous. *In situ* laser-ablation ICP-MS U–Pb dating of titanite indicates short duration of mafic alkaline magmatism in the OWC, lasting from 123.7 ± 2.1 to 117.9 ± 1.8 Ma. Emplacement of the TAR is correlated with the maximum lithospheric thinning that triggered adiabatic decompression and partial melting of the upwelling asthenospheric mantle. Magmatism ceased most likely due to transition to the dominantly compressive regime associated with the major stress field reorganization directly preceding the Carpathian–Alpine Orogeny.

Keywords: mafic alkaline magmatism, teschenite, picrite, Outer Western Carpathians, laser ablation U–Pb titanite dating.

Introduction

The Teschenite Association Rocks (TAR) in the Outer Western Carpathians (OWC) at the Polish–Czech border belong to rather numerous manifestations of the Cretaceous–Cenozoic mafic alkaline volcanism in Europe (Rock 1982; Wilson & Downes 1991; Rossy et al. 1992; Cebriá & Wilson 1995; Spišiak & Balogh 2002; Harangi et al. 2003; Miranda et al. 2009; Spišiak et al. 2011; Matýsek et al. 2018). The TAR form a classic suite of melano- to mesocratic alkaline intrusions emplaced within the OWC flysch named *teschenites* by Hohenegger (1861). Tschermak (1866) coined the term *picrite* for olivine-bearing teschenites distinguishing them from the dominant olivine-free teschenites. Rosenbusch (1887) further classified teschenites as analcime-bearing essexites and analcime-free theralites. The subsequent studies distinguished many more petrographic varieties of the TAR which resulted in further discoveries of teschenite variations (Smulikowski 1929, 1980; Mahmood 1973; Kuděláková 1987; Hovorka & Spišiak 1988; Narębski 1990; Dostal & Owen 1998; Harangi et al. 2003; Włodyka 2010; Matýsek et al. 2018). According to QAPF classification, the TAR correspond to analcime gabbro (LeMaitre et al. 1989).

Rare petrogenetic studies linked the TAR to Jurassic–Early Cretaceous rifting within the southern margin of the European Plate and partial melting of HIMU (high $^{238}\text{U}/^{204}\text{Pb}$)-type mantle source (Dostal & Owen 1998; Harangi et al. 2003). Although there is some uncertainty about the exact timing and duration of the TAR magmatism, stratigraphic criteria and radiometric dating broadly constrain the emplacement time between Valanginian and Cenomanian (Kuděláková 1987; Lucińska-Anczkiewicz et al. 2002; Grabowski et al. 2003; Harangi et al. 2003; Szopa et al. 2014). Thus, the TAR provide a valuable insight into mantle composition, geodynamics and lithospheric processes in the complex paleo-tectonic setting directly preceding formation of the Alpine–Carpathian Orogen.

In this study we review previously published geochemical and isotopic data, and further constrain composition, geochronology and likely petrogenesis of the Teschenite Association Rocks. Besides the previously conducted Sr and Nd isotope studies, we also apply Hf isotope analyses which provide a new insight into the genesis of TAR. We give detailed characteristics of all main petrographic types along with geochemical modelling of partial melting and magma differentiation processes. Additionally, our *in situ* U–Pb titanite dating

results demonstrate short duration of the TAR emplacement during the early Aptian.

Regional geology

The current structure of the OWC was shaped mainly by the Early/Middle Miocene collision of the Alcapa Block with the southern margin of the European Plate during which predominantly Late Jurassic to Early Miocene shelf and deep water flysch deposits with minor carbonates were thrust northward over the Miocene molasse deposits of the Carpathian foredeep (Nemčok et al. 1989; Rögl 1996; Sperner et al. 2002). The suture zone is correlated with the Pieniny Klippen Belt (PKB), which is a narrow, E–W trending zone formed mainly by the Triassic to Oligocene sediments, predominantly carbonates with subordinate fragments of ophiolites deformed in a transpressive setting due to oblique, generally south directed, subduction of the oceanic crust (Birkenmajer 1977, 1986; Nemčok et al. 1989). The PKB separates paleo-accretionary prism of the OWC to the north from the southerly units of the Internal Carpathian chain (Fig. 1a).

Igneous rocks in the OWC are scarce and volumetrically minor. Rare example of continental intraplate magmatic activity is represented by the TAR whose occurrence is limited to the western part of the Silesian Nappe composed of the Upper Jurassic to Miocene, predominantly flysch sediments with subordinate volcaniclastic rocks (Fig. 1b).

The vast majority of the TAR in Poland (Silesia region) occurs in the Valanginian–Hauterivian Upper Cieszyn Beds comprising mainly marls and shales. The Moravian TAR, in the Czech Republic, occur in the Upper Hauterivian–Barremian sandstones and conglomerates of the Těšín–Hradiště Beds and, very rarely, in the Upper Cieszyn Beds and Cieszyn Limestones (Oszczypko 2006).

Teschenites form centimetres to tens of meters thick hypabyssal intrusions (predominantly sills), rarely volcanic flows. They display numerous petrographic and geochemical types ranging from ultrabasic picrites to intermediate teschenites and syenites. Although the radiometric dating results broadly confirm their Early Cretaceous age deduced from the stratigraphic data, they differ substantially when it comes to exact timing and duration of emplacement. The first dating using Ar–Ar method on kaersutite gave ages indicating short duration of magmatism from 122.3 ± 3.2 to 120.4 ± 2.6 Ma (Lucińska-Anczkiewicz et al. 2002). The subsequent K–Ar and U–Pb dating resulted in highly scattered ages suggesting much longer time of the TAR emplacement during Valanginian to Barremian–Aptian (Grabowski et al. 2003; Harangi et al. 2003; Szopa et al. 2014; Matýsek et al. 2018).

Sampling and methods

We present the analyses of 21 TAR samples from 10 locations in the Czech Republic and 5 locations in Poland (Table 1,

Fig. 1b). The whole-rock powders and the heavy-mineral separates were prepared by commonly used techniques of crushing, sieving, magnetic and the heavy liquids separation. About 2–10 kg of rock was first crushed to gravel size in a jaw crusher and then split until 50–100 g of representative whole-rock portion was achieved. This was powdered in an automated agate mortar and subsequently used for geochemical and isotopic analyses. The remaining part of a sample was further crushed to a fraction $<315\text{ }\mu\text{m}$ from which heavy minerals were separated using tetrabromomethane followed by diiodomethane. The final steps involved magnetic separation and handpicking under the stereo microscope.

Whole-rock geochemistry

Geochemical analyses were carried out commercially at the Acme Analytical Laboratories in Canada (<http://acmelab.com>). Samples were first fused with lithium tetraborate and subsequently brought into solution by digestion in nitric acid. Abundance of major elements was determined using ICP-ES while minor and trace elements were measured using ICP-MS (package LF200). Exceptions were Mo, Cu, Pb, Zn and Ni which were first digested in 1:1:1 $\text{HNO}_3:\text{HCl}:\text{H}_2\text{O}$ mixture and measured by ICP-MS.

Mineral chemistry

Chemical composition of the selected minerals was determined using the Cameca SX-100 electron microprobe at the Faculty of Geology, University of Warsaw. The natural and synthetic standards used during analyses were: albite, apatite, diopside, orthoclase, rutile, rhodonite, zircon, barite, tugtupite, Fe_2O_3 , Cr_2O_3 , La-glass, Pr-glass, $\text{CeP}_5\text{O}_{14}$, Nb, NiO , V_2O_5 , ThO_2 , UO_2 , HfO_2 . We applied 15 kV accelerating voltage, 10–20 nA sample current and 1–5 μm beam diameter (larger beam size was applied to mica and feldspar). Integration time at the peak was 10 s and the background was measured for 5 s. The ZAF method was used for correcting the matrix effects.

U–Pb titanite geochronology

Geochronological analyses were carried out in Kraków Research Centre, Institute of Geological Sciences, Polish Academy of Sciences.

In situ U–Pb titanite dating was performed using an excimer laser (ArF) *RESolution M-50* by Resonetics (now Applied Spectra) equipped with a large format, dual-volume sample cell S155 coupled with the ICP-MS *XSeriesII* by ThermoFisher. Titanite crystals were mounted in an epoxy resin and polished. Prior to analyses, a mount was cleaned using acetone, followed by 1N nitric acid and ultra-pure water. Ablation took place in pure He which was mixed in an ablation funnel with Ar nebulizer gas. Downstream, nitrogen was added to enhance sensitivity of the ICP-MS. Before entering ICP source, aerosol passed through a signal smoothing manifold. Basic tuning of

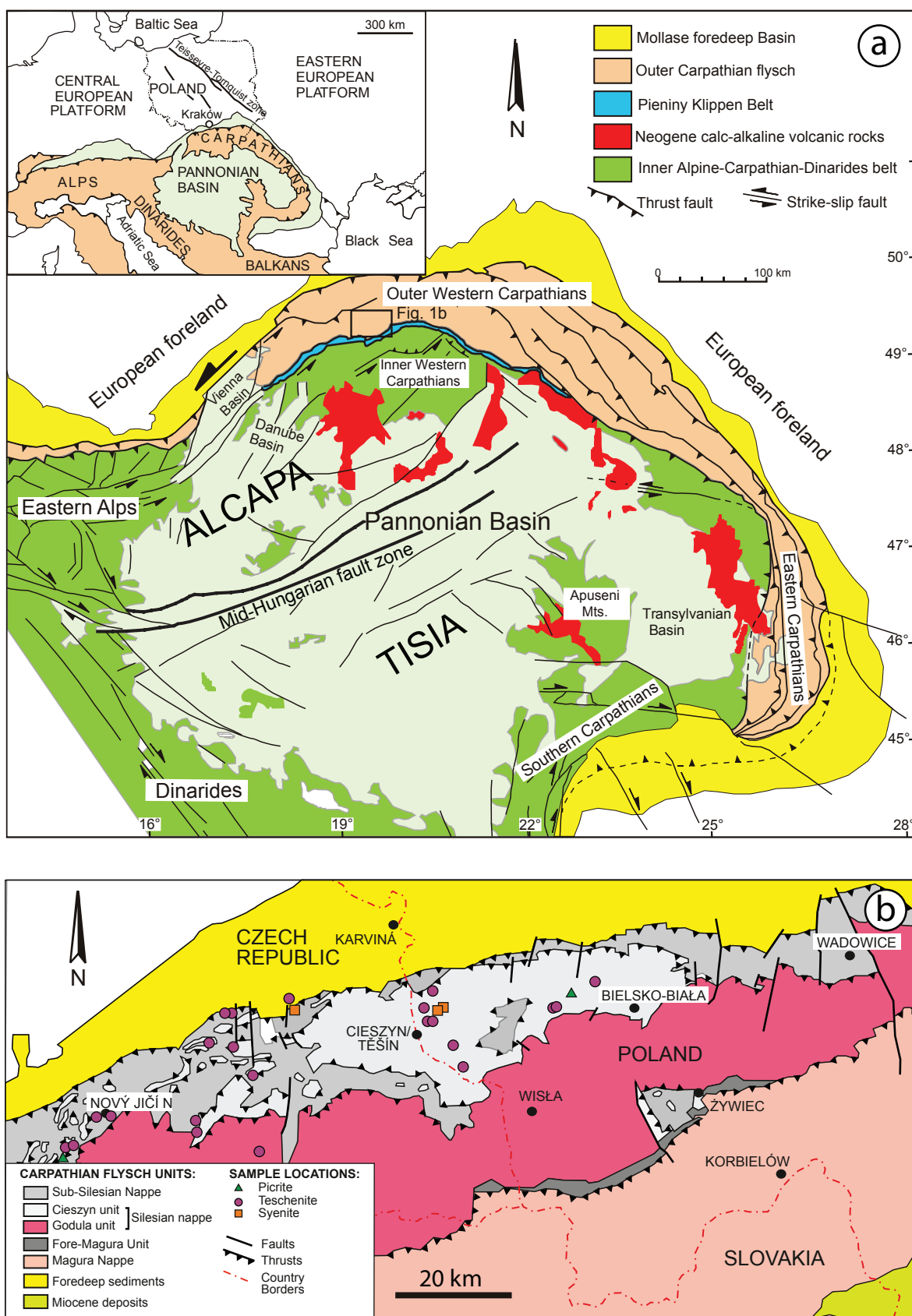


Fig. 1. Simplified geological map of the Carpathian-Pannonian region (a) after Horváth (1993). Small rectangle in (a) marks the Western Carpathian region expanded in (b) after Žytko et al. (1989) with the marked sample locations.

the instrument was conducted using NIST 612 glass standard ablated in a raster mode. Gas flows and torch position were adjusted to maximum signal stability and oxide production below 0.5 % (measured with $^{248}\text{ThO}^+ / ^{232}\text{Th}^+$).

We used 1014.8±2.0 Ma old OLT1 titanite (Kennedy et al. 2010) as a primary standard and 520±5 Ma titanite from Stjernøy in Northern Norway (Pedersen et al. 1989) as a secondary standard. Every six unknowns or the secondary standards, two measurements of the primary standard were carried out. After two cleaning shots, the residual signal was washed out for 30 s and then 35 s of gas blank was measured which was followed by 40 s ablation. Standards and unknowns were ablated using 40 µm spot size and the cleaning shots were of 60 µm diameter. Laser fluence of about 2 J/cm² was applied with ablation frequency of 5 Hz. Summary of the analytical parameters is presented in Table 2.

Data reduction was conducted using Vizual Age_UcomPbne (Chew et al. 2014) in Iolite v. 3.4 program (Paton et al. 2011) functioning under IgorPro software by Wavemetrics. Final age calculations were performed using Isoplot 4.15 (Ludwig 2012). All intercept ages were calculated using common Pb composition estimated applying model of Stacey and Kramers (1975). All reported age errors are 2σ.

Isotope geochemistry

Isotope composition measurements of Sr, Nd and Hf were acquired in the same laboratory as U–Pb titanite dating described above. Sample dissolution, column chemistry and mass spectrometric procedures are outlined in Anczkiewicz & Anczkiewicz (2016) and references therein. Isotope ratio measurements were conducted using multicollector inductively coupled plasma mass spectrometer (MC ICP-MS) *Neptune* by ThermoFisher. Instrumental mass bias of all measured isotopic ratios was corrected using exponential law of Russell et al. (1978). Isotopic ratios of Sr were normalized to $^{87}\text{Sr}/^{86}\text{Sr}=0.1194$, and initial $^{87}\text{Sr}/^{86}\text{Sr}$ ratios were calculated using decay constant $\lambda_{87\text{Rb}}=1.3972\times 10^{-11} \text{ yr}^{-1}$ (Villa et al. 2015). Repeated measurements of the SRM 987 standard over the period of analyses gave $^{87}\text{Sr}/^{86}\text{Sr}=0.710258\pm 12$ (n=7). Mass bias of Nd isotope ratios was corrected by normalization to $^{146}\text{Nd}/^{144}\text{Nd}=0.7219$. The JNd-1 standard yielded $^{143}\text{Nd}/^{144}\text{Nd}=0.512103\pm 9$ (n=6) over a period of analyses. Constants used for the initial $\epsilon(\text{Nd})_i$ calculations: decay constant $\lambda_{147\text{Sm}}=6.54\times 10^{-12} \text{ yr}^{-1}$ (Lugmair and Marti 1978), present-day $^{143}\text{Nd}/^{144}\text{Nd}_{\text{CHUR}(0)}=0.512637$ and $^{147}\text{Sm}/^{144}\text{Nd}_{\text{CHUR}(0)}=0.1966$ (Jacobsen & Wasserburg 1980). Neodymium depleted mantle model age T_{DM} calculations followed DePaolo (1981).

Table 1: GPS coordinates, modal composition and the intensity of secondary alterations of the Teschenite Association Rock samples.

TAR type	Sample	GPS coordinates	Primary mineral assemblage	Secondary alterations
Picrites	CPR-1	N 49°31.584' E 17°57.662'	Ol-Am-Bt-Cpx-(Ap)	x
	CM-1	N 49°50.15' E 18°55.11'	Cpx-Bt-Fs/Fd-(Ap)	xxxx
Teschenites	CSTa-2	N 49°41.281' E 18°16.248'	Cpx-Am-Bt-Fs/Fd-(Ap)	x
	CBS-1	N 49°38.400' E 18°21.966'	Cpx-Bt-Fs-(Ap)	x
	CS-4	N 49°47.419' E 18°53.255'	Cpx-Am-Fs/Fd-(Ap)	xx
	CR-6	N 49°47.70' E 18°38.45'	Cpx-Fs-Bt-(Ap-Ttn)	x
	CP-4	N 49°43.230' E 18°40.110'	Cpx-Am-Bt-Fs/Fd-(Ap-Ttn)	o
	CRE-3	N 49°43.726' E 18°18.349'	Cpx-Am-Fs/Fd-(Ap-Ttn)	x
	CT-1	N 49°34.257' E 18°13.442'	Cpx-Am-Bt-Fs/Fd-(Ap-Ttn)	xxx
	CJ-1	N 49°31.813' E 17°58.190'	Cpx-Am-Bt-Fs/Fd-(Ap-Ttn)	xx
	CBL-1	N 49°34.256' E 18°00.791'	Cpx-Am-Bt-Fs/Fd-(Ap)	x
	CR-1	N 49°47.70' E 18°38.37'	Cpx-Am-Fs/Fd-(Ap)	o
	CRE-2	N 49°43.572' E 18°18.700'	Cpx-Am-Bt-Fs/Fd-(Ap)	x
	CR-8	N 49°47.70' E 18°38.45'	Cpx-Am-Fs/Fd-(Ap-Ttn)	xx
	CHB-1	N 49°44.900' E 18°25.947'	Cpx-Am-Fs/Fd-(Ap)	xx
	CP-3	N 49°43.230' E 18°40.110'	Cpx-Am-Bt-Fs/Fd-(Ap-Ttn)	x
	CB-2	N 49°45.49' E 18°37.80'	Cpx-Am-Fs/Fd-(Ap-Ttn)	x
	CZ-1	N 49°34.527' E 18°02.799'	Fs/Fd-Am-Bt-(Ap)	xxxx
Syenites	CB-4	N 49°46.11' E 18°37.00'	Cpx-Fs-(Ap)	xxxx
	CB-5	N 49°46.11' E 18°37.00'	Cpx-Fs-(Ap)	xxxx
	CZI-1	N 49°44.063' E 18°26.879'	Fs/Fd-Cpx-(Ap-Ttn)	xxx

Minor or accessory minerals are indicated in parentheses. The degree of secondary alterations: o — fresh rock, x — small, xx — medium, xxx — strong, xxxx — very strong. Teschenite CP-1* was exceptionally highly altered with no primary rock-forming minerals preserved, and thus it was used only for titanite dating. Abbreviations: Cpx — clinopyroxene, Am — amphibole, Bt — dark mica, Fs — feldspar, Fd — feldspathoid, (Ap) — accessory apatite, (Ttn) — accessory titanite.

Table 2: Instrument parameters and analytical conditions of laser-ablation ICP-MS analyses.

U–Pb dating	
Laser ablation	RESOlution M-50
Wavelength	193 nm (ArF)
Pulse length	20 ns
Fluence at sample	2 J/cm ²
Repetition rate	5 Hz
Spot size	40 µm
Mass spectrometer	ICP MS XseriesII
RF power (W)	1400
Sample gas Ar flow (L/min)	c. 0.8
Cool gas Ar flow (L/min)	13
Auxiliary gas Ar flow (L/min)	c. 0.9
Nitrogen flow (mL/min)	5–6
He flow (L/min)	c. 0.3
Background measurements (s)	40
Ablation time (s)	40
Washout time (s)	35
Scanned masses	^{43}Ca , ^{206}Pb , ^{207}Pb , ^{208}Pb , ^{232}Th , ^{238}U
Dwell time (ms)	5, 50, 50, 30, 30, 20

Hafnium isotope ratios were normalized to $^{179}\text{Hf}/^{177}\text{Hf}=0.7325$. Values used for the initial $\epsilon(\text{Hf})_i$ calculations: decay constant $\lambda_{176\text{Lu}}=1.865\times 10^{-11} \text{ yr}^{-1}$ (Scherer et al. 2001), present day $^{176}\text{Hf}/^{177}\text{Hf}_{\text{CHUR}(0)}=0.282785$ and $^{176}\text{Lu}/^{177}\text{Hf}_{\text{CHUR}(0)}=0.0336$ (Bouvier et al. 2008). The JMC475 Hf standard gave $^{176}\text{Hf}/^{177}\text{Hf}=0.282160\pm 13$ (n=8) over the period of analyses.

Table 3: Major (wt. %) and trace element (ppm) concentrations of the Teschenite Association Rocks.

Rock type: Sample no.:	Picrite		Tescheneite										
	CPR-1	CM-1	CSTa-2	CBS-1	CS-4	CR-6	CP-4	CRE-3	CT-1	CJ-1	CBL-1	CR-1	CRE-2
SiO ₂	39.8	37.79	42.16	42.22	40.97	42.38	43.24	45.58	37.74	38.89	40.6	41.33	41.52
TiO ₂	0.96	1.92	2.32	2.77	2.09	3.15	3.02	2.69	3.83	2.91	3.15	2.79	3.03
Al ₂ O ₃	4.45	6.21	9.72	12.36	11.66	11.97	12.94	16.67	11.26	14.19	15.15	17.7	14.27
Fe ₂ O _{3T}	12.71	12.27	8.47	9.86	11.51	10.51	10.61	9.89	14.57	10.86	12.76	11.57	10.68
MnO	0.2	0.2	0.14	0.15	0.16	0.15	0.14	0.17	0.25	0.19	0.2	0.18	0.13
MgO	28.33	17.87	13.83	7.8	8.97	8.49	7.16	3.99	6.41	5.73	5.45	4.66	7.01
CaO	4.5	12.45	15.65	14.32	14.21	16.44	14.94	7.77	11.89	12.6	12.47	10.06	11.7
Na ₂ O	0.54	0.4	1.14	1.53	2.88	1.68	2.04	5.21	1.99	3.44	3.29	2.32	1.77
K ₂ O	0.64	1.42	1.14	2.74	1.06	1.19	2	2.55	2.38	1.61	1.93	3.27	2.45
P ₂ O ₅	0.18	1.42	0.37	0.71	1.02	0.45	0.55	0.96	1.76	1.07	0.75	0.8	0.67
LOI	6.8	7.1	4.3	5.1	4.9	3.2	2.8	4.1	7.3	7.9	3.6	4.8	6.30
Total	99.11	99.05	99.24	99.56	99.43	99.61	99.44	99.58	99.38	99.39	99.35	99.48	99.53
Mg#	72.1	71.5	66.8	68.5	70.6	69.3	69.5	68.6	74.4	69.8	72.1	70.7	69.5
TOT/C	0.11	0.17	0.36	0.51	0.4	0.03	<0.02	0.02	1.08	1.14	0.02	0.05	0.40
TOT/S	0.08	0.09	0.07	0.48	0.16	<0.02	0.12	0.04	0.41	0.21	<0.02	0.06	0.12
<i>LILE</i>													
Cs	0.5	1.1	0.5	1.7	3.6	1.9	5.3	3.5	1.8	3.2	0.3	2.7	1.8
Rb	18.5	25.9	37	53.7	25.7	22.5	57.5	45.8	60	39.3	34.7	66.2	61.5
Ba	246	1138	1025	1046	805	412	995	1106	1009	1195	1023	1211	994
Sr	248.2	912.7	726.7	730.3	1293.6	621.3	1389.9	1028.8	1411.3	1737.2	2251.4	1814.5	1070.3
<i>HFSE</i>													
Th	1.9	11.9	5	6.5	10.2	5	6	10	9.5	15.5	7.2	9.3	9.2
U	0.6	3.6	1.6	1.9	3	1.1	1.6	3.3	2.9	4.5	1.7	1.6	2.9
Nb	25.6	118.5	47.3	77.1	80.4	54	64.6	116.7	117.5	134.5	102.2	106.5	91.5
Ta	1.3	5.5	2.8	4.6	4.4	3.2	4	6.7	7.2	7.3	5.9	6.5	5.5
Pb	1.5	6.2	2.1	3	3.9	3.1	2.4	5.2	4.8	5.7	3	3	3.80
Zr	62.6	337.2	154.7	198.9	192.5	196.6	197	272.1	494.6	380.8	208.5	212.4	242.4
Hf	1.6	6.8	4.5	4.9	4.1	5.5	5.3	5.6	12.4	7.2	4.5	4.1	5.4
Y	8.6	28.5	17.6	24.3	31.7	21.9	23.2	31.4	44.1	31.9	26.7	23.5	28.0
<i>REE</i>													
La	18.5	99.7	37.7	56.3	87.5	41	47.9	77.4	103.4	107	67.8	67	61.7
Ce	31	181.3	68.8	108.8	157.5	78.8	86.4	146	209.7	193.7	122.3	119.5	115.6
Pr	3.48	19.86	7.82	12.54	16.68	9.21	10.19	15.85	25.48	19.89	13.11	12.64	12.92
Nd	14	75.4	31.2	51.6	61.7	37.4	42.2	60.4	102.1	74	51.4	46.2	48.7
Sm	2.49	13.19	6.23	10.04	10.95	7.81	8.6	10.82	19.36	13.03	9.38	8.39	9.38
Eu	0.76	3.85	2.00	3.11	3.55	2.39	2.84	3.49	5.91	4.07	2.93	2.76	3.03
Gd	2.42	10.95	5.68	8.66	9.44	7.1	8.04	9.69	15.91	10.71	8.01	7.45	8.52
Tb	0.34	1.35	0.8	1.16	1.33	0.96	1.09	1.43	2.12	1.42	1.14	1.01	1.21
Dy	1.79	6.29	4.25	6.15	6.64	4.99	5.48	7.12	10.91	7.15	6.34	5.27	6.09
Ho	0.32	1.04	0.75	1.06	1.23	0.9	0.97	1.31	1.87	1.23	1.13	0.93	1.09
Er	0.75	2.56	1.74	2.4	3.05	2.12	2.41	3.18	4.4	3.13	2.81	2.49	2.70
Tm	0.11	0.32	0.24	0.32	0.41	0.27	0.32	0.42	0.58	0.41	0.37	0.37	0.35
Yb	0.61	1.77	1.3	1.76	2.32	1.65	1.9	2.43	3.21	2.32	2.22	1.98	2.15
Lu	0.09	0.23	0.19	0.25	0.32	0.22	0.24	0.36	0.44	0.31	0.31	0.27	0.30
<i>Transition metals</i>													
Cr	855.3	431.1	845.0	78.7	143.7	23.9	47.9	<0.002	<0.002	<0.002	<0.002	<0.002	
Co	105.2	63.7	37.6	36.3	42.4	37	36.4	24.3	37.2	33.5	42.6	36.8	37.8
Ni	709.3	638.2	90.7	20.8	108.7	21.6	20	1.3	27	26.2	17.9	11.2	26.6
Sc	14	15	57	23	22	47	30	4	16	9	11	6	16
V	131	164	225	246	207	305	276	167	226	270	336	289	286
Cu	17.2	144	42.7	58.8	59.7	71.2	58.5	15.6	93.6	69.7	57.2	52.7	73.80
Zn	69	119	34	78	79	55	40	72	147	106	51	45	72.00
Ga	6.9	11.6	13.5	15.6	15.5	16.4	17.8	20.3	21.6	20.6	18.7	18.9	18.4
Sn	<1	3	1	2	2	3	2	2	4	1	1	1	2
W	2.2	1.6	<0.5	<0.5	2.7	2	0.5	3.8	1.9	1.3	2.1	0.7	3.2
Mo	1.4	0.5	2.3	2.1	4.3	0.2	1.3	1.8	1.8	3.8	0.7	0.9	2.3

Table 3 (continued): Major (wt. %) and trace element (ppm) concentrations of the Teschenite Association Rocks.

Rock type: Sample no.:	Teschenite					Syenite		
	CR-8	CHB-1	CP-3/11	CB-2	CZ-1	CB-4	CB-5	CZI-1
SiO ₂	41.74	41.92	43.29	46.83	41.56	47.63	47.04	48.92
TiO ₂	2.67	2.66	2.91	2.21	3.5	2.29	2.28	3.13
Al ₂ O ₃	17.07	15.68	13.01	17.1	14.27	15.03	15.13	13.91
Fe ₂ O _{3T}	11.05	11.8	11.44	7.69	11.21	10.28	9.84	12.76
MnO	0.19	0.2	0.17	0.13	0.16	0.13	0.13	0.16
MgO	4.12	4.78	6.75	4.47	4.55	5.45	5.09	4.22
CaO	10.7	10.03	14.17	8.17	7.31	6.97	7.89	6.40
Na ₂ O	2.81	4.31	2.09	4.42	4.63	4.4	4.46	4.65
K ₂ O	2.47	2.32	1.93	2.77	1.05	1.57	1.64	1.59
P ₂ O ₅	0.97	1.19	0.67	0.07	1.04	0.39	0.38	0.45
LOI	5.70	4.60	3.10	5.70	10.20CZ	5.50	5.80	3.05
Total	99.49	99.49	99.53	99.56	99.48	99.64	99.68	99.69
Mg-no.	70.0	70.9	70.5	65.8	70.2	68.5	69.0	72.1
TOT/C	0.04	0.02	0.04	0.07	1.73	0.28	0.5	0.15
TOT/S	<0.02	0.10	0.15	0.06	0.16	0.04	0.12	<0.02
<i>LILE</i>								
Cs	3.9	0.8	2.9	9.6	4.2	2.8	3.5	0.8
Rb	50	47.5	45.5	49.9	23.2	25.2	25.9	27.3
Ba	1120	1197	829	1325	735	748	845	644
Sr	1650.7	1077.1	597	545.5	1321.5	1003.5	951.9	727.4
<i>HFSE</i>								
Th	8.6	11.8	7.0	10.4	9.0	3.0	2.9	4.4
U	1.8	3.8	1.6	2.9	1.7	0.1	0.9	1.5
Nb	103.1	108.9	84.5	129.7	113.6	37.9	36.9	51.3
Ta	6.7	6.1	5.0	8.6	7.0	2.2	2.4	3.2
Pb	3.20	4.40	3.00	13.9	2.50	2.40	1.90	2.30
Zr	209.5	223.5	204.5	260.7	396.4	130.8	126.4	191.1
Hf	4.2	4.4	5.0	5.1	8.6	3.4	3.3	4.6
Y	26.0	29.6	25.4	20.3	33.5	19.0	18.3	26.0
<i>REE</i>								
La	74.1	93.1	58.7	53.7	82.1	26.1	25.4	43.0
Ce	134.5	158.0	106.5	92.1	162.5	48.3	47.2	77.5
Pr	14.25	16.81	11.94	9.87	18.56	5.87	5.63	8.78
Nd	53.6	62.3	47.5	34.7	73.1	24.7	24.0	35.2
Sm	9.45	10.93	8.96	6.08	13.49	5.33	5.25	7.32
Eu	2.98	3.48	3.00	2.03	4.22	1.92	1.86	2.39
Gd	8.08	9.33	7.99	5.52	11.44	5.32	5.18	7.24
Tb	1.14	1.27	1.11	0.82	1.60	0.80	0.77	1.07
Dy	5.90	6.80	5.83	4.58	8.43	4.18	4.07	5.40
Ho	0.97	1.15	1.00	0.85	1.44	0.79	0.81	0.99
Er	2.41	2.87	2.48	2.14	3.49	1.97	1.96	2.51
Tm	0.34	0.39	0.35	0.30	0.45	0.26	0.24	0.32
Yb	2.02	2.40	1.90	1.87	2.42	1.41	1.39	2.01
Lu	0.29	0.32	0.27	0.24	0.33	0.19	0.19	0.27
<i>Transition metals</i>								
Cr	<0.002	<0.002	88.9	27.4	<0.002	13.7	13.7	<0.002
Co	34.6	38.9	38.3	22.6	24.4	32.1	32.6	34.5
Ni	7.3	9.4	21.4	13.2	11.1	40.3	43.8	22.4
Sc	5	5	26	25	7	16	15	16
V	274	261	268	175	215	175	173	254
Cu	38.9	39.3	66.6	28.5	55.1	63.6	64.3	133.1
Zn	63	66	63	95	107	83	81	111
Ga	18.7	19.7	18.1	16.7	21.9	16.5	16.2	18.0
Sn	2	2	2	2	2	2	1	2
W	1.5	1.5	3.2	0.8	1.9	1.3	2.0	1.9
Mo	0.4	1.6	0.4	0.8	3.2	0.4	0.8	0.6

Petrography and mineral chemistry

The Teschenite Association Rocks show wide range of compositional and textural variations (Table 3 and Fig. 2) on a regional, as well as on a single intrusion scale (see also Smulikowski 1929, 1980; Mahmood 1973; Kudělásková 1987; Hovorka & Spišák 1988; Narębski 1990; Dostál & Owen 1998; Harangi et al. 2003; Włodyka 2010; Matýsek et al. 2018). Well-preserved samples, generally, are panidiomorphic, fine- to coarse-grained and have porphyritic, microporphyritic or ophitic textures. Phenocrysts are clinopyroxene, amphibole, olivine, biotite, phlogopite and feldspar. Matrix has composition similar to the phenocrysts but may also contain altered glass and secondary analcime. Apatite and Fe-Ti oxides occur as minor or accessory minerals. Below we present petrography of the main rock types that were subjected to the detailed geochemical, isotopic and geochronological studies. Due to high degree of alterations, precise classification is often problematic, and thus, we applied simplified subdivision distinguishing three main lithological types: 1) ultramafic picrite, 2) the most common, mesocratic teschenite, and rich in felsic minerals 3) mesocratic syenite. Electron microprobe analyses of the selected phenocrysts are presented in Supplementary Table S1.

Picrites (CPR-1, CM-1) are relatively rare and typically poorly preserved. Fairly fresh picrite represented by sample CPR-1 consists mainly of olivine, Ca-amphibole (Ti-rich pargasite and Ti-rich ferro-pargasite), clinopyroxene (diopside), phlogopite, spinel, apatite and opaque minerals (Table S1). Olivine ($Fo_{82}-Fo_{85}$) has CaO content >0.3 wt. % which rules out the direct mantle origin (Simkin & Smith 1970; Sato et al. 1991). Poikilitic amphibole, with no signs of recrystallization or alteration, surrounds smaller crystals of olivine and diopside (Fig. 2a). This indicates that the sample is a cumulate and amphibole probably represents intercumulus liquid of nephelinic composition consolidated around cumulus

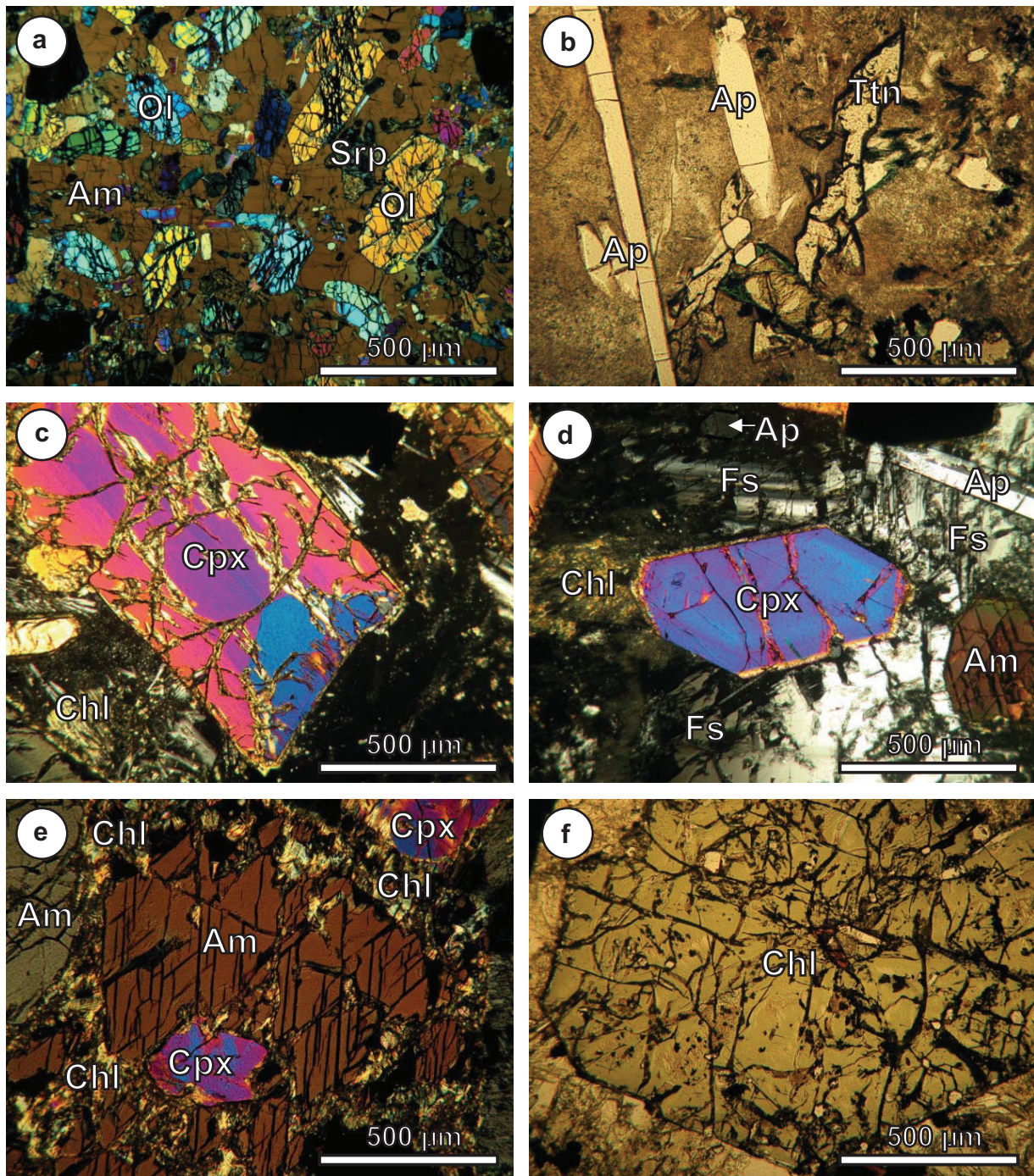


Fig. 2. Photomicrographs of the TAR samples: **a** — olivine enclosed in a large amphibole in picrite CPR-1 (XPL); **b** — elongated apatite and titanite in fine-grained matrix, teschenite CT-1 (PPL); **c** — sector zoning and partial chloritization of clinopyroxene in teschenite CRE-2 (XPL); **d** — clinopyroxene and amphibole surrounded by feldspars, in syenite CZI-1 (XPL); **e** — partly chloritized amphibole with clinopyroxene inclusion in teschenite CR-6 (XPL); **f** — chlorite pseudomorph after pyroxene in syenite CB-4 (PPL). Abbreviations: Am — amphibole; Chl — chlorite; Cpx — clinopyroxene; Ol — olivine; Srp — serpentine; Fs — feldspar; Ttn — titanite; Ap — apatite. XPL — cross polarized light; PPL — plane-polarized light. See text for details.

composed of olivine, spinel, and clinopyroxene (Best 1970; Dawson 1982). Secondary alterations are expressed as chloritization of phlogopite and serpentinization of olivine. Locally, rare carbonate crystals were observed. Unlike CPR-1, picrite CM-1 is severely altered. It comprises relics of clinopyroxene

with numerous olivine inclusions pseudomorphosed by serpentine, phlogopite, apatite and opaque minerals.

The studied teschenites are fine- to coarse-grained, typically with porphyritic textures. Phenocrysts are formed by clinopyroxene, amphibole and dark mica set in fine crystalline matrix

composed of the same minerals with an addition of alkali feldspars, and the secondary analcime. Apatite and opaques occur as minor or accessory minerals. Idiomorphic apatite crystals are common inclusions in the phenocrysts and in matrix (Fig. 2b). In some samples accessory amount of titanite is present (Fig. 2b). Clinopyroxene of diopside composition, locally with hedenbergite rims (Table S1), forms idiomorphic crystals often exhibiting sector zoning (Fig. 2c). In some samples, it occurs as radial aggregates with younger generation overgrowing the earlier diopside. Amphibole frequently overgrows diopside or dark mica and displays wide range of compositions. Typically, it shows rimward increase in Fe, Ti, Si accompanied by decrease in Mg. The core composition corresponds to kaersutite while rim is formed by ferro-pargasite, hastingsite or ferro-kaersutite (Table S1). Rare dark mica crystals are of biotite–annite composition (Table S1). Feldspars are represented chiefly by K-feldspar, albite and rare K–Na-feldspar. Feldspars are commonly carbonatized. Partial chloritization of amphibole is also frequently observed (Fig. 2d).

The most felsic type of the TAR is represented by rare syenites (CZI-1, CB-4, CB-5) characterized by considerably lower mafic phenocrysts/matrix ratio. Phenocrysts are represented by clinopyroxene (diopside, seldom augite) and amphibole (kaersutite, Table S1). Matrix is composed of K-feldspar, albite and secondary analcime (Fig. 2e). Clinopyroxene and amphibole crystals are corroded or partly chloritized along edges and fractures or even entirely chloritized (Fig. 2f). Chlorite aggregates occur also between feldspar crystals. Ilmenite, Fe-oxides and titanite form skeletal and needle-shaped aggregates. Small apatite crystals are abundant as inclusions in feldspar and in the phenocrysts.

In addition to alterations described above, saussuritization and zeolitisation are observed. More detailed account on secondary processes in the TAR can be found in Dolníček et al. (2010a,b, 2012).

Major and trace elements

The chemical composition of the studied samples is given in Table 3. Despite careful sample selection, some degree of alteration is an inherent feature of the TAR which is reflected by the secondary alterations described above but also by the elevated LOI observed in majority of the collected samples (3–7 wt. % with an exception of CZ-1 where LOI is as high as 10.2 wt. %).

The studied samples are generally poor in silica (41–51 wt. % volatile-free) and rich in P_2O_5 and TiO_2 (Fig. 3a, Table 3). CIPW-normative compositions show that TAR are, only with a few exceptions (CB-4, CZI-1, CT-1), strongly silica-under-saturated (normative nepheline up to 15 wt. %). The content of MgO is 4–28 wt. % and $Mg\# = (MgO/(MgO+FeO)) \times 100$ (in molar proportions) varies from 40 to 82 (Table 3).

According to TAS classification (Le Bas et al. 1986) they are mainly basanites or tephrites with smaller number of picropicbasalts, basaltic trachyandesites, basalts and one sample classifies as a phonotephrite (Fig. 3a). Because the degree of major element mobility linked to the secondary alterations has not been quantified, which may cast some doubts on accuracy of this classification, we additionally present classification based on “immobile” trace elements following Pearce (1996). In the latter classification the studied and the previously published teschenites fall within the alkaline fields of alkali basalts, trachybasalts, tephrites, basanites and, similarly to TAS classification, one sample falls within the phonotephrite field (Fig. 3b). Thus, both classifications are largely consistent (Fig. 3a and b).

In the Fenner-type variation diagrams of major-element oxides vs. MgO , two distinct trends are revealed. An inflected trend is observed for CaO and TiO_2 , while Al_2O_3 and Na_2O show a gently curved, convex-downward trend. The remaining oxides (SiO_2 and P_2O_5) do not follow any obvious regular pattern (Fig. 4).

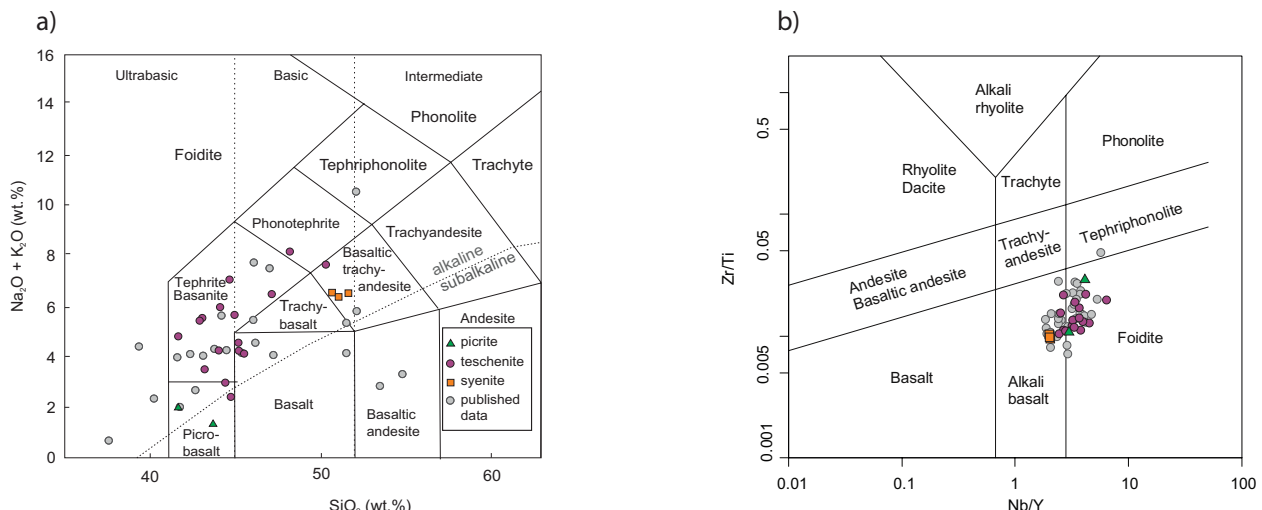


Fig. 3. a — Total Alkali Silica classification diagram (Le Bas et al. 1986); **b** — Nb/Y vs. Zr/Ti classification of Pearce (1996) for the studied TAR (coloured symbols) and the published data shown in grey (Dostál & Owen 1998; Harangi et al. 2003; Włodyka 2010).

All samples show mutually comparable abundances of trace elements, with an exception of picrite CPR-1 that displays significantly lower trace-element contents (Fig. 5). However, all samples display generally strong enrichment in incompatible over more compatible elements expressed as a negative slope in primitive-mantle normalized spider diagram (Fig. 5a). A little smaller degree of enrichment is observed for the syenites (Fig. 5a). Besides the negative slope, other features common

for our samples are: negative Rb, K, Pb and Hf anomalies, positive Nb, Ta, Ba, LREE and, less conspicuous, Sr anomaly (Fig. 6a). Similarly chondrite-normalized REE diagram displays sub-parallel, linear patterns with high enrichment in more incompatible light REE ($\text{La}_n/\text{Yb}_n = 12-38$) and no Eu anomalies (Fig. 5b). In absolute values, light REE enrichment is the highest in the picrites and the lowest in the syenites. Heavy REE show very low normalized values and display

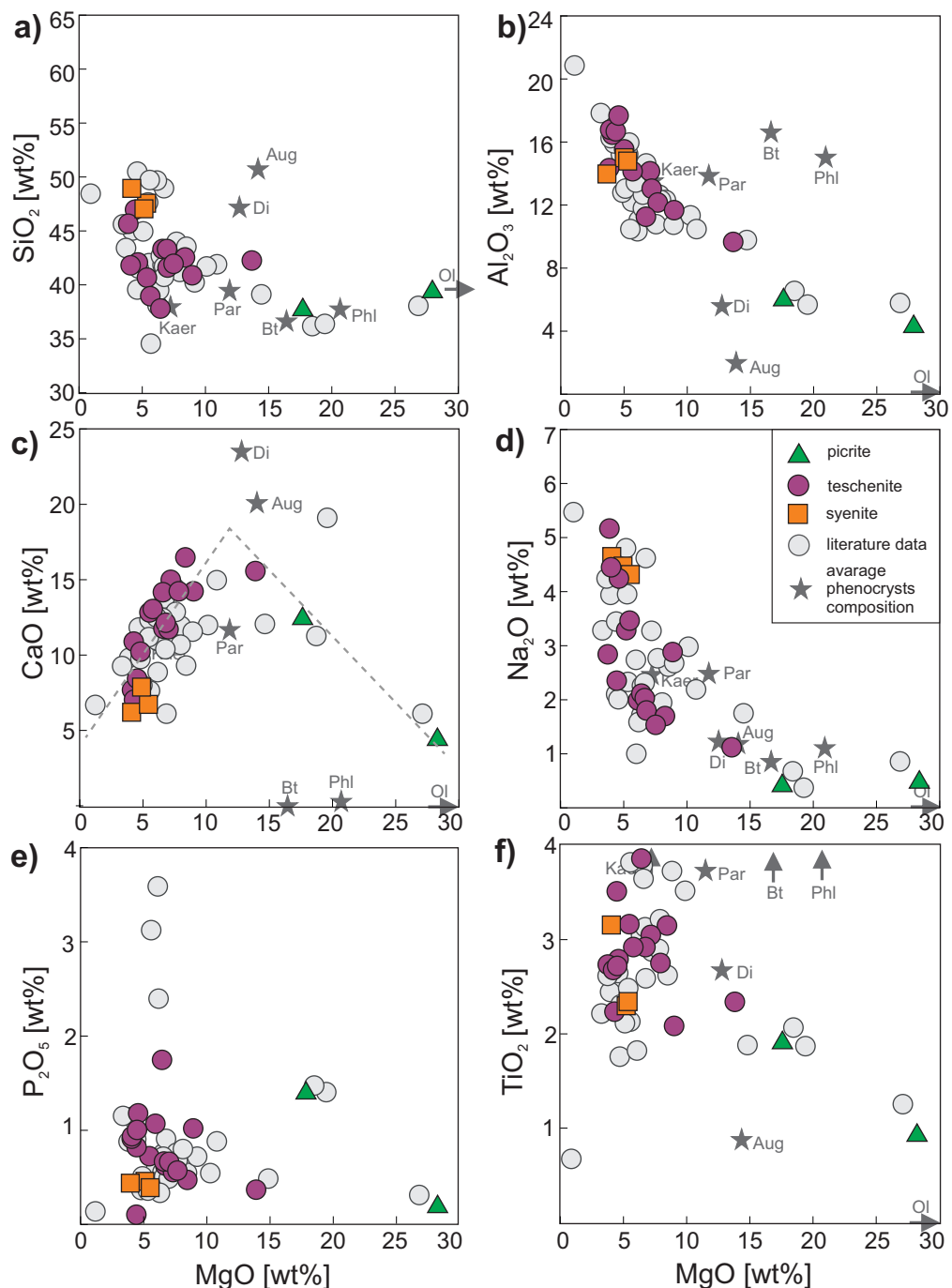


Fig. 4. Fenner diagrams of MgO vs.: a — SiO_2 ; b — Al_2O_3 ; c — CaO ; d — Na_2O ; e — P_2O_5 and f — TiO_2 . The previously published data shown in grey (Dostal & Owen 1998; Harangi et al. 2003; Włodyka 2010). Average chemical composition of the phenocrysts according to the microprobe analyses presented in Table S1. Abbreviations: Aug — augite; Di — diopside; OI — olivine; Kaer — kaersutite; Par — paragonite; Bt — biotite; Phl — phlogopite.

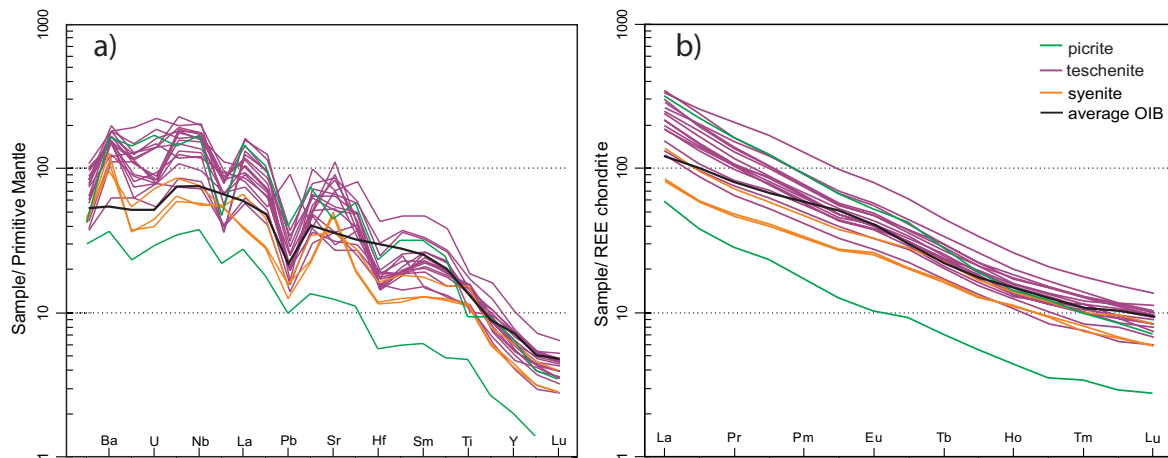


Fig. 5. Spider diagrams: **a** — primitive-mantle normalized trace-elements, normalization values after McDonough & Sun (1995); **b** — chondrite-normalized REE, normalization values after Boynton (1984). Average ocean island basalt (OIB) composition after Sun & McDonough (1989).

much less variations in abundance in comparison to that observed for light REE.

Laser-ablation ICP-MS U–Pb titanite dating

The dating results obtained for six samples are summarized in the Supplementary Table S2 and Fig. 6. Each sample was analyzed during an individual session during which the secondary standard measurements were accurate within $\leq 1\% \text{ 2 RSD}$ (2 relative standard deviations) and yielded the weighted mean age of $520.9 \pm 3.5 \text{ Ma}$ ($\text{MSWD}=2.0, n=7$).

We analyzed 20–40 crystals depending on abundance of titanite in a sample. Expectedly, the analyses show significant and variable amounts of common Pb. Crystals virtually common Pb-free are scarce and were found only in sample CHB-1 from Horní Bludovice (Fig. 6). Nevertheless, the obtained dating results reveal a rather coherent picture. Intercept ages with Terra-Wasserburg concordia and ^{207}Pb -corrected weighted mean ages show slight variations but are indistinguishable within the estimated uncertainties.

Five out of six samples gave nearly identical lower intercept ages between 117.9 ± 1.8 and $119.3 \pm 1.4 \text{ Ma}$ ($\text{MSWD} < 2$ for all samples). Only teschenite CT-1 from Tichá yielded an older age of $123.7 \pm 2.1 \text{ Ma}$ (Fig. 6) which was confirmed by a replicate measurement. Due to a high closure temperature of the U–Pb system in titanite (e.g., Villa 1998; Cherniak 2000) and very fast cooling of small bodies emplaced into a cold shallow crust, we interpret the obtained ages as reflecting the time of intrusive TAR emplacement.

Isotope geochemistry

Whole-rock Sr, Nd and Hf isotope compositions are presented in Table 4. Initial $^{143}\text{Nd}/^{144}\text{Nd}$ and $^{176}\text{Hf}/^{177}\text{Hf}$ ratios (corrected for emplacement age $t=120 \text{ Ma}$) yielded a very

narrow range of $\epsilon(\text{Nd})_i=5.0$ to 6.3 and wider range of $\epsilon(\text{Hf})_i=4.9$ to 10.0 shown in Figure 7a–b. This results in a steep array in $\epsilon(\text{Nd})_i-\epsilon(\text{Hf})_i$ diagram, intersecting the Terrestrial Array of Vervoort et al. (2011). Unlike Nd and Hf isotopes, $^{87}\text{Sr}/^{86}\text{Sr}_i$ initial ratios vary broadly from 0.7032 to 0.7071 (Fig. 7a).

Discussion

Fractional crystallization

Except for the cumulate picrite CPR-1, the other samples of the TAR do not fulfil the requirements for mantle primary partial melts, and thus they must have undergone some degree of differentiation (Green & O'Hara 1971; Gill 2010). The significance of fractional crystallization (FC) process is suggested by the presence of geochemical trends showing higher variations in compatible relatively to incompatible trace elements (Fig. 8) and the presence of cumulate texture in picrite CPR-1. The inflected trend in the MgO–CaO diagram (Fig. 4c) implies that the magmas were most likely subjected to two stages of differentiation: (1) CaO increase probably related to olivine crystallization, and (2) CaO decrease likely related to fractionation of clinopyroxene. The first stage could have led to the formation of relatively primitive teschenites (e.g. CS-4) and the second fractionation step would have led to the formation of the more evolved teschenites and syenites. The negative correlations of MgO vs. Na_2O , Al_2O_3 and SiO_2 , as well as the absence of Eu anomaly suggest that feldspar fractionation did not play any significant role in TAR formation (Figs. 4 and 5b).

Crustal contamination

Trace-element ratios sensitive to crustal contamination (e.g., Th/La, Zr/Nb, Ba/Nb, La/Nb) along with Nb/Yb vs. Th/Yb discrimination diagram of Pearce (2008) shown in Fig. 9a

argue against the significant crustal involvement in the magma genesis of the TAR. Similarly, narrow range of positive $\epsilon(\text{Nd})_i = 5.0\text{--}6.3$ and $\epsilon(\text{Hf})_i = 4.9\text{--}10.0$ point to very little, if any, crustal contamination (see also Dostal & Owen 1998; Harangi et al. 2003). High and diverse $^{87}\text{Sr}/^{86}\text{Sr}$ values (Fig. 7a), which typically point to the crustal involvement, are most likely a result of interaction with the Nd-poor and Sr-rich liquids, possibly sea or diagenetic water (Rossy et al. 1992; Dolníček et al. 2010b).

Partial melting

High enrichment in incompatible elements, $\text{Zr}/\text{Nb}=2.0\text{--}4.2$, $\text{K}/\text{Nb}<179$, decreasing La/Yb ratios with increasing SiO_2

content along with the positive $\epsilon(\text{Nd})_i$ and $\epsilon(\text{Hf})_i$ values, imply that parental magmas may have formed by the small degree of partial melting of a mantle source (Fig. 9b). TiO_2/Yb vs. Nb/Yb diagram of Pearce (2008) points to a rather deep, garnet peridotite melting (Fig. 9c). The presence of the residual garnet in the source is also suggested by the low HREE content and strong light to heavy REE fractionation (Fig. 5b).

Using the GCDkit (Janoušek et al. 2006, 2016) and PETROMODELER software (Ersøy 2013), we conducted modelling of non-modal batch melting adapting initial mantle source composition of Clague & Frey (1982) together with the modified modal garnet and spinel peridotite compositions of Bradshaw et al. (1993). We used the distribution coefficients

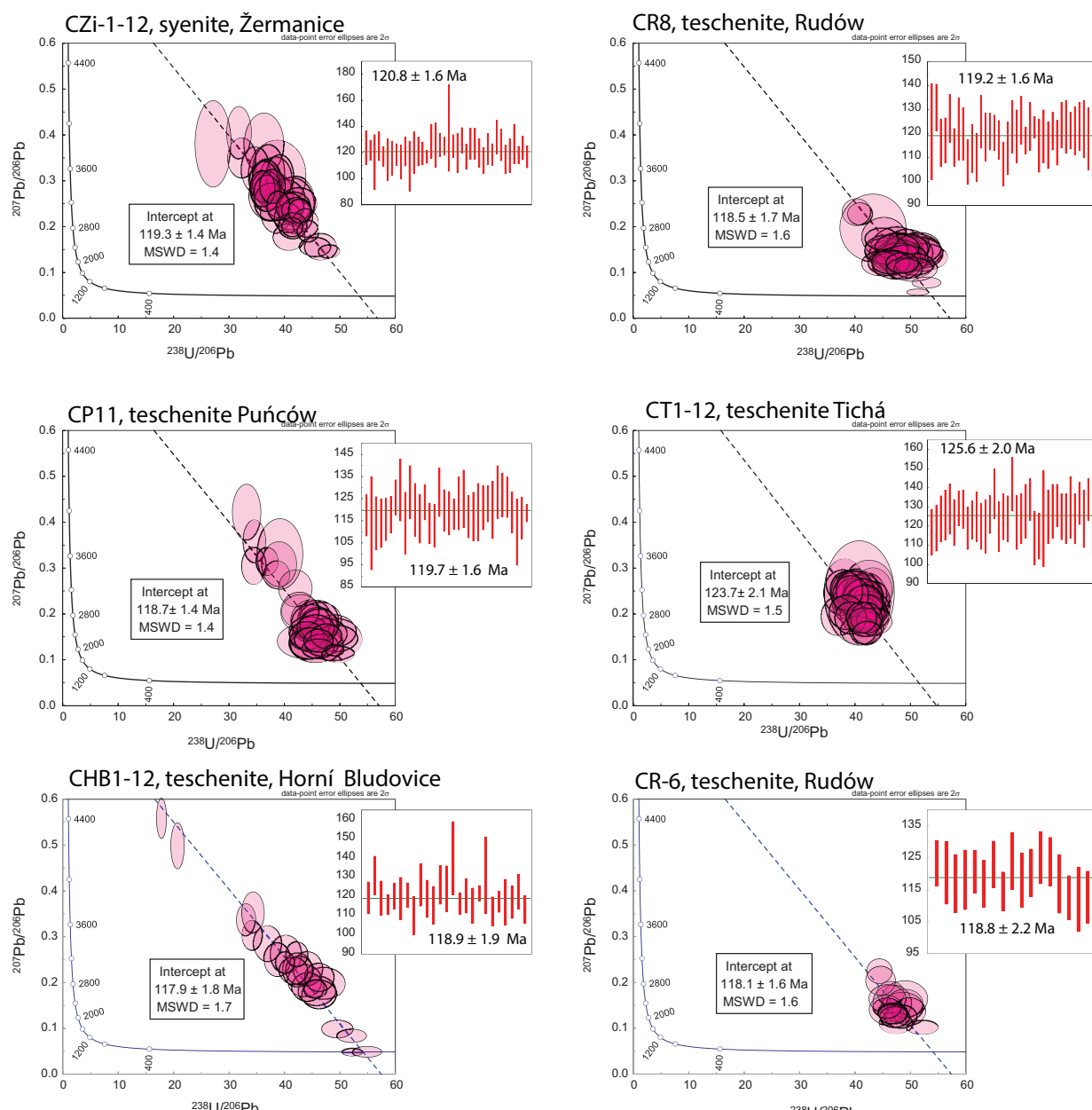


Fig. 6. Laser-ablation ICP-MS U-Pb titanite dating results. Ellipses represent 2σ errors.

Table 4: Summary of Rb–Sr, Sm–Nd and Lu–Hf isotope analyses of the Teschenite Association Rocks. Initial $^{87}\text{Sr}/^{86}\text{Sr}_i$ ratios, $\varepsilon(\text{Nd})_i$ and $\varepsilon(\text{Hf})_i$ calculated for emplacement time $t=120$ Ma.

Sample	Lithology	Sm [ppm]	Nd [ppm]	$^{147}\text{Sm}/^{144}\text{Nd}$	$^{143}\text{Nd}/^{144}\text{Nd}$	$\varepsilon\text{Nd}_{(120)}$	T _{DM} Nd (Ga)	Rb [ppm]	Sr [ppm]	$^{87}\text{Rb}/^{86}\text{Sr}_*$	$^{87}\text{Sr}/^{86}\text{Sr}$	$^{176}\text{Lu}/^{177}\text{Hf}$	$^{176}\text{Lu}/^{177}\text{Hf}$	$\varepsilon\text{Hf}_{(120)}$			
CPR-1	picrite	2.65	13.11	0.1221	0.512879±4	5.9	0.30	18.5	248.2	0.2051	0.703562±16	0.703218	0.09	1.63	0.0082	0.282985±5	9.1
CM-1	picrite	14.02	79.20	0.1071	0.512834±7	5.2	0.32	25.9	912.7	0.0781	0.704200±10	0.704069	0.24	7.16	0.0048	0.282858±5	4.9
CSFa-2	teschenite	6.45	30.68	0.1271	0.512864±9	5.5	0.34	37.0	726.7	0.1401	0.704025±13	0.703790	0.19	4.43	0.0062	0.282944±6	7.8
CBS-1	teschenite	10.17	48.03	0.1280	0.512863±10	5.4	0.35	53.7	730.3	0.2024	0.703719±11	0.703379	0.23	4.92	0.0067	0.282933±5	7.4
CS-4	teschenite	11.31	62.79	0.1089	0.512877±10	6.0	0.27	25.7	1293.6	0.0547	0.703700±10	0.703608	0.34	4.25	0.0112	0.282998±5	9.3
CR-6	teschenite	8.04	38.92	0.1250	0.512869±6	5.6	0.33	22.5	621.3	0.1139	0.703737±11	0.704949	0.23	5.84	0.0056	0.282973±4	8.9
CP-4	teschenite	9.21	41.74	0.1334	0.512882±9	5.8	0.34	57.5	1390	0.1225	0.705140±12	0.703775	0.24	5.38	0.0064	0.282963±5	8.4
CRE-3	teschenite	11.54	61.72	0.1131	0.512850±9	5.4	0.32	45.8	1029	0.0997	0.703981±11	0.703570	0.34	5.84	0.0083	0.282961±5	8.2
CT-1	teschenite	18.50	94.80	0.1180	0.512834±8	5.0	0.36	60.0	1411	0.1170	0.703856±12	0.703660	0.41	12.34	0.0048	0.282930±6	7.4
CJ-1	teschenite	12.95	73.11	0.1071	0.512830±8	5.1	0.33	39.3	1737	0.0424	0.704137±8	0.706056	0.32	7.29	0.0061	0.282943±5	7.8
CBL-1	teschenite	9.20	49.01	0.1134	0.512863±7	5.7	0.30	34.7	2251	0.1582	0.706127±12	0.704500	0.31	4.63	0.0095	0.283007±6	9.8
CRE-2	teschenite	9.46	48.94	0.1169	0.512847±9	5.3	0.33	61.5	1070	0.0623	0.704765±9	0.704033	0.29	5.49	0.0074	0.282950±6	7.9
CR-8	teschenite	10.09	56.06	0.1088	0.512856±8	5.6	0.30	50.0	1651	0.1214	0.704536±9	0.704031	0.29	4.29	0.0095	0.282984±7	9.0
CHB-1	teschenite	10.62	60.19	0.1067	0.512848±9	5.5	0.30	47.5	1077	0.0833	0.704235±12	0.704396	0.32	4.35	0.0103	0.282970±5	8.4
CP-3	teschenite	9.14	46.28	0.1194	0.512870±8	5.7	0.31	45.5	597.0	0.2098	0.705755±11	0.705403	0.27	5.13	0.0076	0.282980±6	9.0
CZ-1	teschenite	13.22	68.85	0.1161	0.512858±8	5.6	0.32	23.2	1322	0.0483	0.703980±11	0.703899	0.32	8.84	0.0051	0.282949±5	8.1
CB-4	syenite	5.58	24.42	0.1383	0.512911±16	6.2	0.30	25.2	1004	0.0691	0.707240±10	0.707124	0.21	3.51	0.0083	0.282999±4	9.6
CB-5	syenite	5.47	23.90	0.1383	0.512909±8	6.2	0.31	25.9	951.9	0.0749	0.706193±11	0.706067	0.20	3.39	0.0085	0.283011±10	10.0
CZ-1	syenite	7.69	70.07	0.0663	0.512858±8	6.3	0.21	27.3	727.4	0.1033	0.704629±8	0.704456	0.28	5.00	0.0078	0.283000±6	9.7

All errors are 2SE (standard errors) and relate to the last significant digits. Concentrations determined by isotope dilution method, except for Rb and Sr which were determined by ICP-MS. Uncertainty of $^{87}\text{Rb}/^{86}\text{Sr}$, $^{147}\text{Sm}/^{144}\text{Nd}$ and $^{176}\text{Lu}/^{177}\text{Hf}$ ratios are 1 %, 0.3 % and 0.5 %, respectively. Normalizing ratios, decay constants, model values used for the calculations along with standards reproducibility are given in the main text.

from Kostopoulos & James (1991). Details of modelling parameters are presented in Table 5.

The calculated melting curves plotted in the Zr/Nb vs. Ce/Y plot (Fig. 10a) show that nearly all samples presented in this study, and the vast majority of the published data, could have originated by 2–5 % partial melting of peridotite containing ca. 2.5 to 6.0 % of garnet (Fig. 10a). Only very few samples reported by Włodyka (2010) show better fit with a curve portraying the partial melting of a spinel-bearing source. Additionally, we calculated melting curves in the $\text{Yb}_n/\text{Ce}_n/\text{Yb}_n$ space which is more sensitive to the presence of garnet and spinel in the source (Fig. 10b). This projection clearly excludes the possibility of melting in the spinel stability field suggested in Fig. 10a and by Harangi et al. (2003). Furthermore, it narrows down the range of garnet content in the source to ca. 4–6 %. At the same time, it suggests slightly wider range of melting fractions from 2.5 to 10 %. However, in this respect, inferences based on Fig. 10a seem more adequate, as Zr/Nb ratio is more sensitive to the degree of partial melting. The subhorizontal shift of some data in the direction of higher Yb_n content seems to be associated with magma differentiation or very the low abundance of garnet, but not with the presence of spinel in the source.

Our modelling results show that the low degree of partial melting of the metasomatized garnet peridotite, with, or without, fractional crystallization, could well explain the trace-element variations in practically all the TAR.

Magma source

Geochemical signature of the TAR places them in the group of alkaline within-plate basalts with distinct OIB affinity as inferred on the basis of the projections shown in Figure 9a and c of Pearce (2008). This is additionally supported by the relative enrichment in the incompatible trace elements (Fig. 5) and, typical of OIB, HFSE ratios such as Zr/Y=7–13, Zr/Nb=2–4 and Nb/Yb=18–76 (Ulrych et al. 1993). The negative anomalies of Rb, K and Pb with the high primitive-mantle normalized Nb and Ta contents (Fig. 5a) further constrain magma source as a HIMU-type OIB (Wilson & Downes 1991). The enrichment in LILE relative to HFSE indicates the presence of an enriched component together with HIMU and the depleted mantle signature (Fig. 11).

Although the HIMU reservoir was initially defined on the basis of the highly radiogenic Pb isotope composition, it is also characterized by the distinct Nd–Hf isotope systematics (Woodhead 1996; Hanyu et al. 2012; Nebel et al. 2013). The HIMU acquired fractionated (Sm–Nd)/(Lu–Hf) relative to

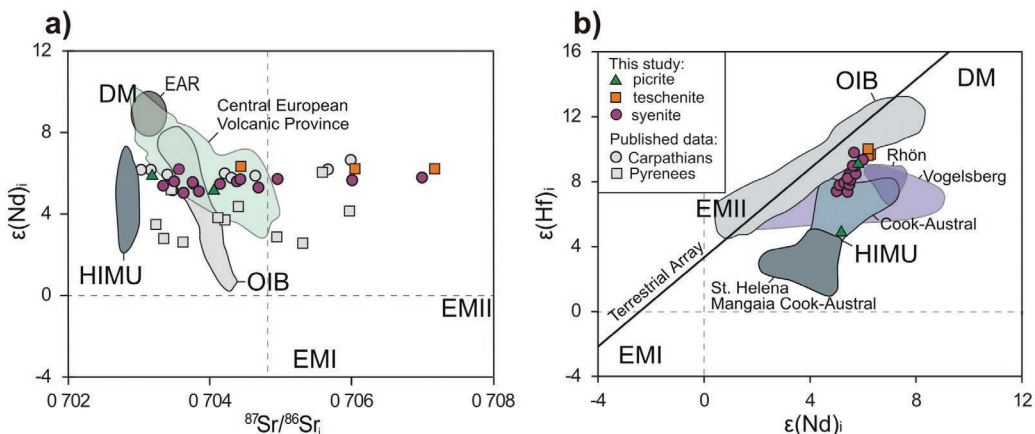


Fig. 7. Sr–Nd–Hf isotope composition of the TAR: **a** — initial $^{87}\text{Sr}/^{86}\text{Sr}_i$ vs. $\epsilon(\text{Nd})_i$ and **b** — initial $\epsilon(\text{Nd})_i$ vs. $\epsilon(\text{Hf})_i$ diagrams. Initial ratios corrected for the emplacement time $t=120$ Ma. Terrestrial Array after Vervoort et al. (2011). Published Sr–Nd isotope data for the Pyrenees from Rossy et al. (1992), for the Carpathians from Dostal & Owen (1998), Harangi et al. (2003), for Central and Western Europe from Wilson & Downes (2006); Nd–Hf isotope data for Vogelsberg area from Jung et al. (2011), for Rhön area from Jung et al. (2005) and Jung & Hoernes (2000), HIMU, OIB, EM, DM data from Woodhead (1996), Chauvel et al. (1997), Salters and White (1998), Hanyu et al. (2012), Nebel et al. (2013). Lower part of the field is shown for the most extreme HIMU signature from St. Helena and Mangaia (Cook–Austral Islands).

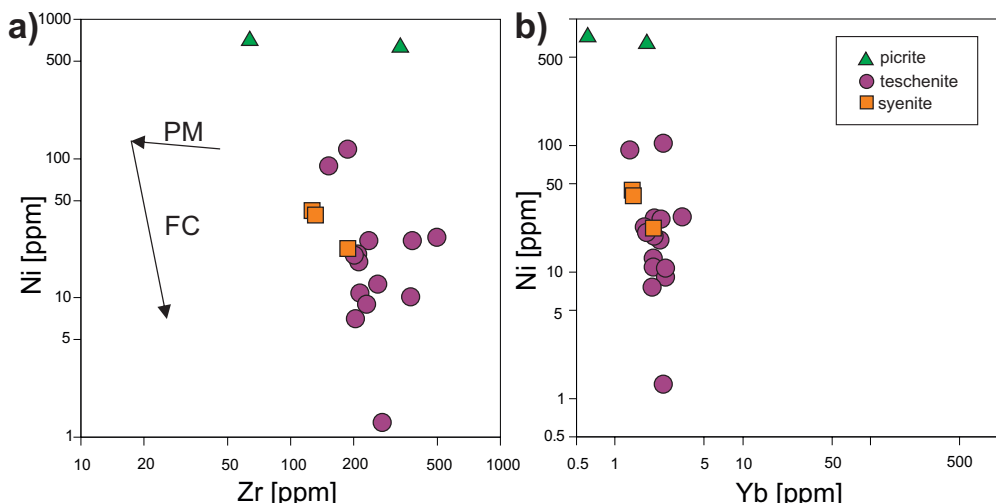


Fig. 8. Log–log diagrams showing relationship between incompatible (Zr, Yb) and compatible (Ni) elements in response to dominantly partial melting (PM) or fractional crystallization (FC) processes, indicated by tentatively estimated vectors: **a** — Zr vs. Ni and **b** — Yb vs. Ni.

the BSE, and thus the HIMU-derived magmatic rocks plot significantly below the Terrestrial Array, forming its own, much steeper linear trend (Fig. 7b). Only sample CM-1 displays the same systematics as typical HIMU rocks from St. Helena and Mangaia (Cook–Austral Islands). The remaining samples lie within, or on the prolongation of the field defined mostly by more radiogenic Cook–Austral samples (Fig. 7b). The most radiogenic TAR fall into the OIB field, close to the Terrestrial Array. Thus, we interpret the observed Nd–Hf isotopic systematics as a result of mixing between components derived from HIMU-type and less fertile component like MORB type basalts (Fig. 7b).

As mentioned above, Sr isotopes are of little use when it comes to constraining petrogenesis of the TAR. However, it is noteworthy that the lowest $^{87}\text{Sr}/^{86}\text{Sr}_i$ coupled with a very narrow range of $\epsilon(\text{Nd})_i$ values seem to converge near the HIMU

field which well agrees with the general picture derived from the Nd–Hf isotopes (Fig. 7a).

Although high concentration of the incompatible elements could be primarily due to the low degree of partial melting, the significant degree of mantle metasomatism is indicated by the abundance of amphibole, apatite or phlogopite even in the most primitive samples. The depletion of K and Rb relative to Ba, Nb and Ta (Fig. 5a) points to the presence of the residual amphibole and/or phlogopite in the mantle source. The dominant role of amphibole is inferred on the basis of high K/Rb (>250) and low Rb/Sr (<0.09) in the melts (Furman & Graham 1999; Ulrych et al. 2011), and on the basis of the common occurrence of this phase in the European mantle xenoliths (Downes 2001). Volatile-rich mantle domains could have originated due to infiltration of subduction-related fluids from the recycled oceanic crust possibly during the Variscan

Orogeny. As also pointed out by Dostal & Owen (1998), this is suggested by the depleted mantle Nd model ages (0.26–0.36 Ga; Table 4). The presence of the recycled oceanic crust at the depth of 400–600 km in the Central European mantle was proposed

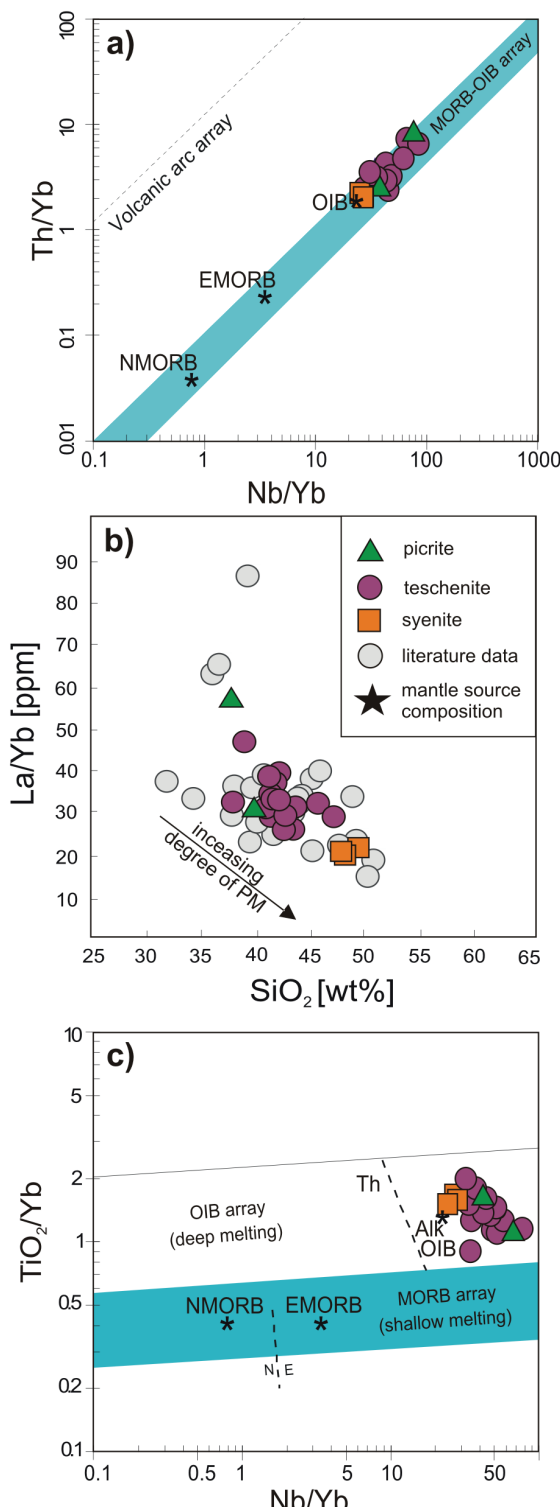


Fig. 9. Incompatible element ratios diagrams: **a** — Nb/Yb vs. Th/Yb (Pearce 2008); **b** — SiO₂ vs. La/Yb; **c** — Nb/Yb vs. TiO₂/Yb (Pearce 2008). Data from the previous studies shown in grey (Dostal & Owen 1998; Harangi et al. 2003; Włodyka 2010).

on the basis of seismic tomography studies (Piromallo et al. 2001).

The presence of the HIMU asthenospheric mantle in Europe is often explained in the context of hot fingers derived from a mantle plume (Wilson & Bianchini 1999). So called “super plume event”, involving mantle upwellings worldwide, started at ca. 120 Ma (Larson 1991), i.e. during the TAR emplacement. Harangi et al. (2003) proposed that Cape Verde plume activity, that triggered central Atlantic opening, could either have channelled the HIMU component in the N–NE direction or pollute the upper mantle layer beneath Europe, leading to the formation of the common European Asthenospheric Reservoir (EAR, Cebriá & Wilson 1995). Mantle plume may have generated mafic, volatile-rich intrusions that caused the upper mantle metasomatism (Bogaard & Wörner 2003; Seghedi et al. 2004a).

An alternative scenario requires transport of the deep mantle material with the HIMU signature to the volatile-rich upper mantle, in response to adiabatic decompression and passive upwelling. Adiabatic decompression rather than mantle plume is our preferred mechanism given the short duration and small volume of TAR volcanism as well as an overall extensional, incipient rift setting in the studied region during Early Cretaceous. Since the volatile-rich mantle domains melt more readily, even small decompression would induce melting. Adiabatic decompression appears to have played a significant role also in generating Cenozoic magmatism in Europe (Wilson & Downes 2006; Lustrino & Wilson 2007).

Timing of TAR emplacement

There have been several attempts of dating alkaline rocks from the OWC. Lucińska-Anczkiewicz et al. (2002) conducted Ar–Ar dating of kaersutites and obtained a tight group of ages for the three mesocratic teschenites, yielding a weighted mean age of 122.3±3.2 Ma. Dating of an additional syenite sample by the same authors gave a little younger, but still overlapping within the analytical precision, age of 120.4±2.6 Ma. This led the authors to a suggestion that the more evolved magma could have intruded slightly later.

These coherent results, suggesting short duration of alkaline magmatism in the area, are in marked contrast to the subsequent geochronological studies. The reported K–Ar ages of amphibole, biotite and whole-rock fractions vary widely from 63.6±1.6 to 148.6±3.6 Ma (Grabowski et al. 2003) and from 96.3±3.7 to 128.3±5.6 Ma (Harangi et al. 2003). Grabowski et al. (2003) explained the wide range of ages as a result of hydrothermal alterations but the oldest, biotite ages spanning from 137.9±2.0 to 133.1±1.8 Ma were interpreted as reliable and reflecting the time of biotite crystallization during teschenites emplacement. Szopa et al. (2014) applied *in situ* LA ICP-MS U–Pb apatite dating that resulted in two rather imprecise ages of 103±20 and 127±9 Ma. The third sample from Pućów gave fairly precise 119.6±3.2 Ma age, confirming earlier Ar–Ar dating results of Lucińska-Anczkiewicz et al. (2002) from the same locality (120.4±2.6 Ma). The recent

U–Pb dating of apatite from the Žermanice sill, using laser ablation multi collector ICP-MS, also provides an imprecise 120 ± 10 Ma age, interpreted as the time of sill emplacement (Matýsek et al. 2018).

High scatter among the published K–Ar ages is almost certainly caused by the well acknowledged excess Ar problems, in the studied area caused, at least partly, by very strong alterations in the vast majority of the TAR. High common Pb in apatite, on the other hand, along with the low U content, are responsible for the low precision of *in situ* U–Pb dating, which

Table 5: Input parameters used for non-modal batch melting modelling shown in Fig. 10. Abbreviations: Ol — olivine, Opx — orthopyroxene, Grt — garnet, Sp — spinel.

Mantle source modal composition and melting modes, modified from Bradshaw et al. (1993)					
%	Ol	Opx	Cpx	Grt	Sp
Proportion of phases					
Spinel peridotite	60	20	15	0	5
Garnet peridotite 2.5 %	60	23	14.5	2.5	0
Garnet peridotite 4 %	60	22.5	13.5	3	0
Garnet peridotite 6 %	60	22.5	11.5	6	0
Contribution to melt					
Spinel peridotite	10	10	50	0	30
Garnet peridotite 2.5 %	10	30	55	5	0
Garnet peridotite 4 %	10	30	55	5	0
Garnet peridotite 6 %	10	30	55	5	0
Trace element composition of mantle source (Clague & Frey 1982)					
ppm	Zr	Nb	Ce	Y	Yb
	20	4	5.44	6	0.6
Partition coefficients (Kostopoulos & James 1992)					
	Zr	Nb	Ce	Y	Yb
Ol	0.1	0.0001	0.000008	0.01	0.0194
Opx	0.03	0.001	0.00105	0.1	0.0631
Cpx	0.16	0.015	0.0389	0.2	0.19
Spl	0.05	0.0001	0.000008	0.0078	0.00032
Grt	0.32	0.04	0.0014	2.2885	4.7

makes such ages of limited use. Taking into account the published interpretations of the previous geochronological studies, teschenites in the Outer Western Carpathians would have been emplaced between 138 and 105 Ma with the most reproducible ages grouping around 105 to 123 Ma. This suggests ca. 20 to even 30 Ma long period of alkaline magmatism during the Early Cretaceous. Our new U–Pb titanite dating of five teschenites and one syenite are in good agreement with the Ar–Ar data of Lucińska-Anczkiewicz et al. (2002). Five out of six samples gave unresolvable within the analytical precision ages between 117.9 ± 1.8 and 119.3 ± 1.4 Ma (Fig. 6). Notably, severe alterations in the teschenite CP-1 from Puńcow did not have any negative consequences for our dating results. The U–Pb system in titanite must have remained intact as indicated by a very good age consistency with the four other samples. Only teschenite CT-1 from Tichá area gave an older 123.7 ± 2.1 Ma age that we interpret as reflecting the earlier emplacement time.

On the whole, our results along with the ages of Lucińska-Anczkiewicz et al. (2002) indicate that small portions of partial melts were extruded, or emplaced into a shallow crust, within a rather short period of time, between 124 and 119 Ma.

Geodynamic implications

The Early Cretaceous to Neogene mafic alkaline rocks from Western and Central Europe show similar geochemical and isotopic systematics (Rossy et al. 1992; Hovorka & Spišiak 1993; Hovorka et al. 1999; Ivan et al. 1999; Harangi 2001; Spišiak & Balogh 2002; Harangi et al. 2003; Seghedi et al. 2004a,b; Wilson & Downes 2006; Jung et al. 2011; Spišiak et al. 2011; Oszczyplko et al. 2012) Wide areal extent of geochemically and isotopically similar igneous activity implies the presence of a relatively long-lived, enriched reservoir in the upper mantle which likely can be correlated with European Asthenospheric Reservoir (EAR) as defined by Cebriá &

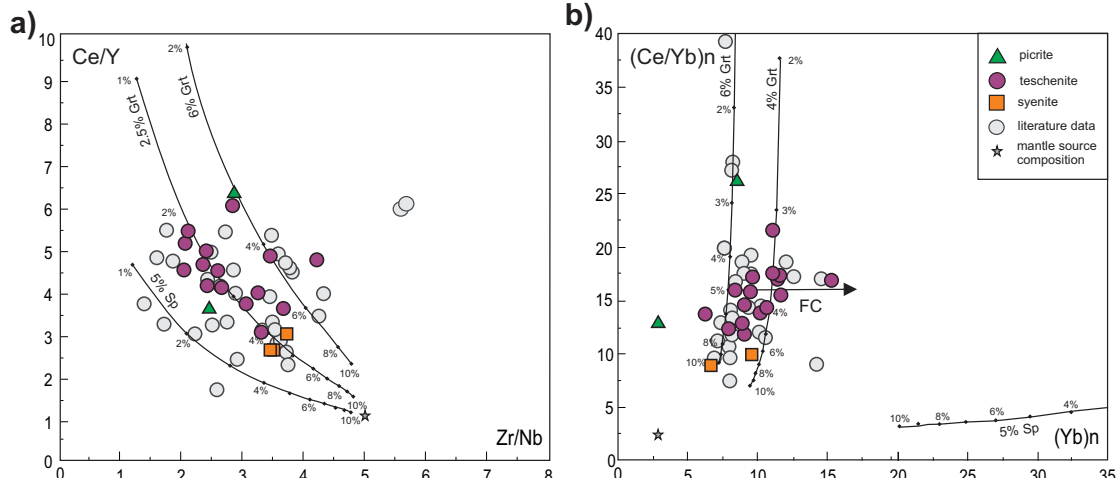


Fig. 10. Trace-elements based petrogenetic partial melting model of the TAR magmas calculated using GCDkit (Janoušek et al. 2006) and PETROMODELLER software (Ersoy 2013). Data from the previous studies shown in grey (Dostál & Owen 1998; Harangi et al. 2003; Włodyka 2010). Modelling parameters summarized in Table 5.

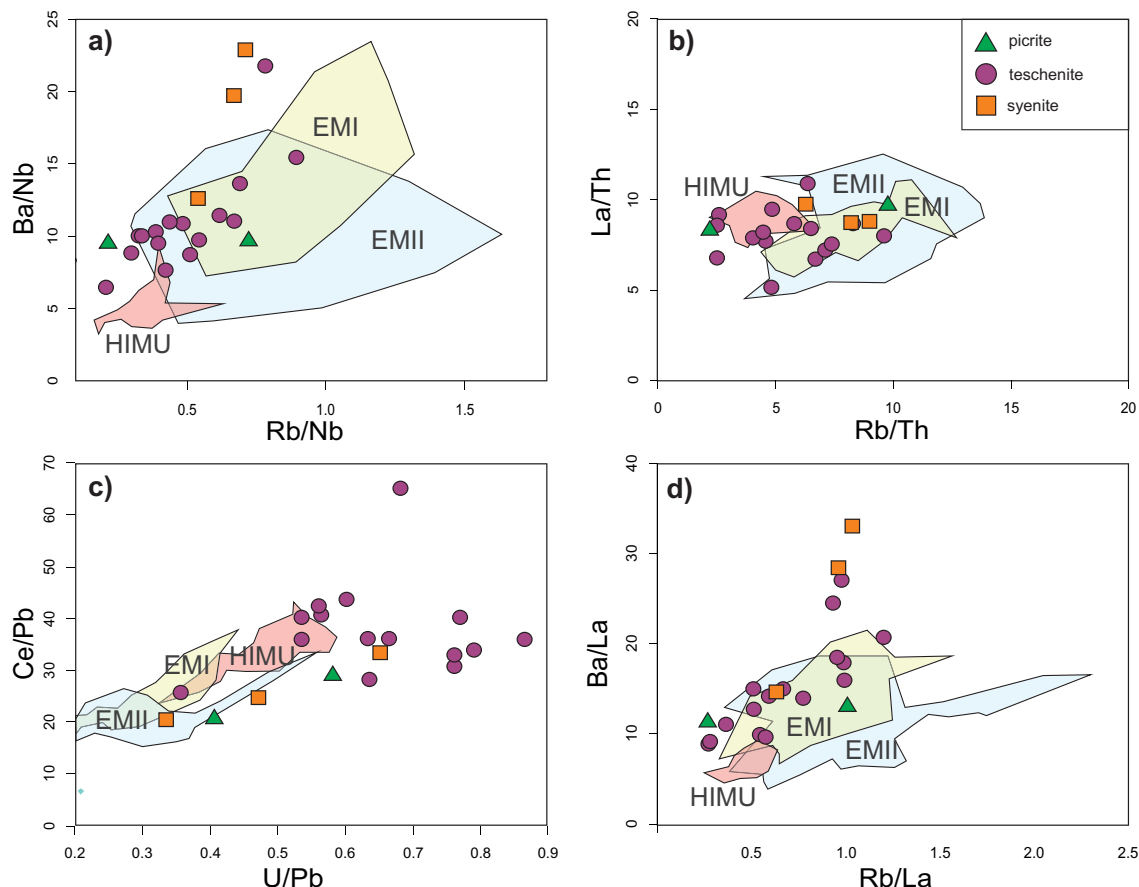


Fig. 11. Trace-element ratio diagrams: **a** — Rb/Nb vs. Ba/Nb; **b** — Rb/Th vs. La/Th; **c** — U/Pb vs. Ce/Pb and **d** — Rb/La vs. Ba/La showing fields characteristic of ocean-island basalts derived from HIMU, EMI and EMII mantle end-members (Willbold & Stracke 2006).

Wilson (1995). Our study of the TAR shows that their petrogenesis, indeed, can be associated with EAR, as also suggested by Harangi et al. (2003). The Cretaceous mafic alkaline volcanism, including volumetrically minor alkaline magmatism in the Outer Western Carpathians, is interpreted as a result of the incipient rift zone formation that triggered opening of the Alpine Tethys and the North Pyrenean Rift Zone. The Teschenite Association Rocks occur exclusively within the Silesian Nappe which constitutes central part of the former Outer Western Carpathians Basin. This basin formed as a result of rifting within the southern passive margin of the European Plate, possibly due to the eastward escape and rotation of the Alcapa and Tisia blocks in the Late Jurassic to Early Cretaceous (Słomka 1986; Ślączka et al. 1999; Spišák et al. 2011). Rift never evolved to a sea-floor spreading stage (Nemčok et al. 2001) and the maximum extent of the Outer Western Carpathians Basin was reached during Hauterivian–Aptian (Książkiewicz 1960). Maximum lithospheric thinning achieved during Early Aptian possibly triggered the adiabatic decompression and the partial melting in the volatile-rich metasomatized asthenospheric mantle. Our dating results indicate that the extension climax was accompanied by short (~ 5 Myr) episode of alkaline magmatism lasting from ca. 124 to 119 Ma. The short duration of the magmatic activity in the Silesian Basin could be related to a major stress

reorganization in the region. The maximum extension that we correlate with the TAR emplacement was followed in the southeastern Outer Carpathians by the compressive regime in the Aptian–Albian (Sandulescu 1988; Kruglov 1989). This compressional phase was also manifested by uplift of the intra-basin ridges, the siliciclastic turbidites deposition and the syn-sedimentary folding in the Silesian and Magura basins (Švábenická et al. 1997; Oszczypko 2006). Hence, it seems plausible to assume that rapid transition from the extensional climax to the compressive regime during the Aptian could have ceased mafic alkaline magmatism in the Silesian Basin.

Conclusions

The Jurassic–Early Cretaceous formation of the rift-related sedimentary basins in the northern part of the Tethys Ocean was accompanied by alkaline magmatism. A suite of the ultrabasic to intermediate Teschenite Association Rocks was emplaced within the Silesian Basin due to small degree of partial melting of the metasomatized asthenospheric mantle likely accompanied by some degree of the two-stage fractional crystallization. Melting was triggered by the maximum lithospheric thinning associated with rifting and adiabatic decompression at the southern margin of the European Plate.

About 2–5 % of partial melting occurred most likely within the volatile-rich mantle domains in the garnet stability field. Mantle metasomatism might have been induced by the earlier, Variscan subduction events. The Nd–Hf isotopic signature, together with the incompatible trace-elements composition, indicate the HIMU-type OIB mantle source mixed with the more “depleted”, probably MORB-type component. The geochemical and isotopic characteristics point to the genesis associated with the European Asthenospheric Reservoir — the common mantle end-member for the widespread Cenozoic volcanic rocks in Europe — that seems important also for the Cretaceous mafic volcanism in Central and Western Europe.

In situ U–Pb titanite dating indicates that the TAR were emplaced over a short period of time between 124 and 119 Ma (Aptian) during maximum lithospheric thinning in the Outer Western Carpathians Basin. Magmatic activity ceased during the major stress reorganization associated with the transition to the dominantly compressive regime between the southern European margin and North Africa.

Acknowledgments: This project was funded by Polish National Science Centre grant no. 2011/01/B/ST10/04683. We thank Zdeněk Dolníček for his help in the field and creative discussions and Jakub Bazarník as well as Dariusz Sala for their laboratory and field assistance. We are grateful to Skár Óyvind and Allen Kennedy for sharing titanite standards. We are indebted to Vojtěch Janoušek and an anonymous reviewer for providing very detailed and helpful reviews. We are grateful to Milan Kohút and Igor Petřík for the editorial handling of the manuscript.

References

- Anczkiewicz A.A. & Anczkiewicz R. 2016: U–Pb zircon geochronology and anomalous Sr–Nd–Hf isotope systematics of late orogenic andesites: Pieniny Klippen Belt, Western Carpathians, South Poland. *Chem. Geol.* 427, 1–16.
- Best M.G. 1970: Kaersutite–peridotite inclusions and kindred megacrysts in basanitic lavas, Grand Canyon, Arizona. *Contrib. Mineral. Petrol.* 27, 25–44.
- Birkenmajer K. 1977: Jurassic and Cretaceous lithostratigraphic units of the Pieniny Klippen Belt, Carpathians, Poland. *Studia Geol. Polon.* 45, 1–159.
- Birkenmajer K. 1986: Stages of structural evolution of the Pieniny Klippen Belt, Carpathians. *Studia Geol. Polon.* 88, 7–32.
- Bogaard P.J.F. & Wörner G. 2003: Petrogenesis of basanitic to tholeiitic volcanic rocks from the Miocene Vogelsberg, Central Germany. *J. Petrol.* 44, 569–602.
- Bouvier A., Vervoort J.D. & Patchett P.J. 2008. The Lu–Hf and Sm–Nd isotopic composition of CHUR: Constraints from unequilibrated chondrites and implications for the bulk composition of terrestrial planets. *Earth Planet. Sci. Lett.* 273, 48–57.
- Boynton W.V. 1984: Cosmochemistry of the Rare Earth Elements: Meteorite Studies. In: Henderson R. (Ed.): Developments in Geochemistry 2. Elsevier, Amsterdam, 63–114.
- Bradshaw T.K.K., Hawkesworth C.J.J. & Gallagher K. 1993: Basaltic volcanism in the Southern Basin and Range: no role for a mantle plume. *Earth Planet. Sci. Lett.* 116, 45–62.
- Cebriá J. & Wilson M. 1995: Cenozoic mafic magmatism in Western/ Central Europe: a common European asthenospheric reservoir. *Terra Nova, Abstract Supplement* 7, 162.
- Chauvel C., McDonough W., Guille G., Maury R. & Duncan R. 1997: Contrasting old and young volcanism in Rurutu Island, Austral chain. *Chem. Geol.* 139, 125–143.
- Cherniak D.J. 2000: Rare earth element diffusion in apatite. *Geochim. Cosmochim. Acta*. 64, 3871–3885.
- Chew D.M., Petrus J.A. & Kamber B.S. 2014: U–Pb LA-ICPMS dating using accessory mineral standards with variable common Pb. *Chem. Geol.* 363, 185–199.
- Clague D.A. & Frey F.A. 1982: Petrology and trace element geochemistry of the Honolulu volcanics, Oahu: implications for the oceanic mantle below Hawaii. *J. Petrol.* 23, 447–504.
- Dawson J.B. 1982: Upper-Mantle Amphiboles: A Review. *Mineral. Mag.* 45, 35–46.
- DePaolo D.J. 1981: Neodymium isotopes in the Colorado Front Range and crust–mantle evolution in the Proterozoic. *Nature* 291, 193–196.
- Dolníček Z., Kropáč K., Uher P. & Poláč M. 2010a: Mineralogical and geochemical evidence for multi-stage origin of mineral veins hosted by teschenites at Tichá, Outer Western Carpathians, Czech Republic. *Chem. Erde-Geochem.* 70, 267–282.
- Dolníček Z., Urubek T. & Kropáč K. 2010b: Post-magmatic hydrothermal mineralization associated with Cretaceous picrite (Outer Western Carpathians, Czech Republic): interaction between host rock and externally derived fluid. *Geol. Carpath.* 61, 327–339.
- Dolníček Z., Kropáč K., Janíčková K. & Urubek T. 2012: Diagenetic source of fluids causing the hydrothermal alteration of teschenites in the Silesian Unit, Outer Western Carpathians, Czech Republic: petroleum-bearing vein mineralization from the Stříbrník site. *Mar. Petrol. Geol.* 37, 27–40.
- Dostal J. & Owen J.V. 1998: Cretaceous alkaline lamprophyres from northeastern Czech Republic: geochemistry and petrogenesis. *Geol. Rundschau* 87, 67–77.
- Downes H. 2001: Formation and modification of the shallow sub-continental lithospheric mantle: a review of geochemical evidence from ultramafic xenolith suites and tectonically emplaced ultramafic massifs of western and central Europe. *J. Petrol.* 42, 233–250.
- Ersoy E.Y. 2013: PETROMODELER (Petrological Modeler): a Microsoft Excel spreadsheet program for modelling melting, mixing, crystallization and assimilation processes in magmatic systems. *Turk. J. Earth Sci.* 22, 115–125.
- Furman T. & Graham D. 1999: Erosion of lithospheric mantle beneath the East African Rift system: geochemical evidence from the Kivu volcanic province. *Lithos* 48, 237–262.
- Gill R. 2010: Igneous rocks and processes. a practical guide, 1st ed. Wiley-Blackwell, Chichester, 1–428.
- Grabowski J., Krzeminski L., Nescieruk P., Szydlo A., Paszkowski M., Pécskay Z. & Wójtowicz A. 2003: Geochronology of teschenitic intrusions in the outer Western Carpathians of Poland — constraints from ⁴⁰K/⁴⁰Ar ages and biostratigraphy. *Geol. Carpath.* 54, 385–393.
- Green D.H. & O’Hara M.J. 1971: Composition of basaltic magmas as indicators of conditions of origin: application to oceanic volcanism [and discussion]. *Philos. T. Royal Soc. A.* 268, 707–725.
- Hanyu T., Tatsumi Y., Senda R., Miyazaki T., Chang Q., Hirahara Y., Takahashi T., Kawabata H., Suzuki K., Kimura J.I. & Nakai S. 2012: Geochemical characteristics and origin of the HIMU reservoir: a possible mantle plume source in the lower mantle. *Geochem. Geophys. Geosys.* 12, 1–30.
- Harangi S. 2001: Neogene magmatism in the Alpine-Pannonian Transition Zone — A model for melt generation in a complex geodynamic setting. *Acta Vulcanol.* 13, 25–39.

- Harangi S., Tonarini S., Vaselli O. & Manetti P. 2003: Geochemistry and petrogenesis of Early Cretaceous alkaline igneous rocks in Central Europe: implications for a long-lived EAR-type mantle component beneath Europe. *Acta Geol. Hung.* 46, 77–94.
- Hohenegger L. 1861: Die geognostischen Verhältnisse der Nordkarpathen in Schlesien und des angrenzenden Theilen von Mähren und Galicien als Erläuterung zu der geognostischen Karte der Nordkarpathen. *Perthes*, Gotha, 1–50.
- Horváth F. 1993: Towards a mechanical model for the formation of the Pannonian basin. *Tectonophysics* 226, 333–357.
- Hovorka D. & Spišiak J. 1988: Mesozoic volcanism of the Western Carpathians. *Veda*, Bratislava, 1–263 (in Slovak).
- Hovorka D. & Spišiak J. 1993: Mesozoic volcanic activity of the Western Carpathian Segment of the Tethyan Belt: diversities in space and time. *Jahrb. Geol. Bundesanst.* 136, 769–782.
- Hovorka D., Dostál J. & Spišiak J. 1999: Geochemistry of the Cretaceous alkali basaltic rocks of the central part of the Western Carpathians (Slovakia). *Krystalinikum* 25, 37–48.
- Ivan P., Hovorka D. & Méres Š. 1999: Riftogenic volcanism in the Western Carpathian geological history: a review. *GeoLines* 9, 41–47.
- Jacobsen S.B. & Wasserburg G.J. 1980: Sm-Nd isotopic evolution of chondrites. *Earth Planet. Sci. Lett.* 50, 139–155.
- Janoušek V., Farrow C.M. & Erban V. 2006: Interpretation of whole-rock geochemical data in igneous geochemistry: introducing Geochemical Data Toolkit (GCDkit). *J. Petrol.* 47, 1255–1259.
- Janoušek V., Moyen J.-F., Martin H., Erban V. & Farrow C. 2016: Geochemical modelling of igneous processes — principles and recipes in R Language, 1st ed. *Springer*, Heidelberg New York Dordrecht London, 1–346.
- Jung S. & Hoernes S. 2000: The major- and trace-element and isotope (Sr, Nd, O) geochemistry of Cenozoic alkaline rift-type volcanic rocks from the Rhön area (central Germany): Petrology, mantle source characteristics and implications for asthenosphere-lithosphere interactions. *J. Volcanol. Geotherm. Res.* 99, 27–53.
- Jung S., Pfänder J.A., Brügmann G. & Stracke A. 2005: Sources of primitive alkaline volcanic rocks from the Central European Volcanic Province (Rhön, Germany) inferred from Hf, Os and Pb isotopes. *Contrib. Mineral. Petrol.* 150, 546–559.
- Jung S., Pfänder J.A., Brauns M. & Maas R. 2011: Crustal contamination and mantle source characteristics in continental intra-plate volcanic rocks: Pb, Hf and Os isotopes from central European volcanic province basalts. *Geochim. Cosmochim. Acta* 75, 2664–2683.
- Kennedy A.K., Kamo S.L., Nasdala L. & Timms N.E. 2010: Grenville skarn titanite: potential reference material for SIMS U-Th-Pb analysis. *Can. Mineral.* 48, 1423–1443.
- Kostopoulos D.K. & James S.D. 1991: Parameterization of the melting regime of the shallow upper mantle and the effects of variable lithospheric stretching on mantle modal stratification and trace-element concentrations in magmas. *J. Petrol.* 33, 665–691.
- Kruglov S. 1989: Geodynamics of the Ukrainian Carpathians. *Geol. Carpath.* 40, 101–123.
- Książkiewicz M. 1960: Pre-orogenic sedimentation in the Carpathian geosyncline. *Geol. Rundsch.* 50, 8–31.
- Kudělasková J. 1987: Petrology and geochemistry of selected rock types teschenite association, Outer Western Carpathians. *Geol. Carpath.* 38, 545–573.
- Larson R.L. 1991: Latest pulse of Earth: evidence for a mid-Cretaceous superplume. *Geology* 19, 6, 547–550.
- Le Bas M.J.L., Maitre R.W.L., Streckeisen A. & Zanettin B. 1986: A chemical classification of volcanic rocks based on the Total Alkali-Silica Diagram. *J. Petrol.* 27, 745–750.
- LeMaitre R.W., Streckeisen A., Zanettin B., LeBas M.J., Bonin B., Bateman P., Bellieni G., Dudek A., Efremova S., Keller J., Lamérye J., Sabine P.A., Schmid R., Sørensen H. & Woolley A.R. 1989: Igneous rocks: a classification and glossary of terms. International Union of Geological Sciences subcommission on the systematics of igneous rocks, 32–39.
- Locock AJ. 2014: An Excel spreadsheet to classify chemical analyses of amphiboles following the IMA 2012 recommendations. *Computers & Geosciences* 62, 1–11.
- Lucińska-Anczkiewicz A., Villa I.M., Anczkiewicz R. & Ślączka A. 2002: ^{40}Ar / ^{39}Ar dating of alkaline lamprophyres from the Polish Western Carpathians. *Geol. Carpath.* 53, 45–52.
- Ludwig K.R. 2012: A geochronological toolkit for Microsoft Excel. *Berkeley Geochronology Center Spec. Publ.* 5, 1–75.
- Lugmair G.W. & Marti K. 1978: Lunar initial ^{143}Nd / ^{144}Nd : differential evolution of the lunar crust and mantle. *Earth Planet. Sci. Lett.* 39, 349–357.
- Lustrino M. & Wilson M. 2007: The circum-Mediterranean anorogenic Cenozoic igneous province. *Earth-Sci. Rev.* 81, 1–65.
- Mahmood A. 1973: Petrology of the teschenitic rock series from the type area of Cieszyn (Teschen). *Ann. Soc. Geol. Pol.* XLIII, 153–216.
- Matýsek D., Jirásek J., Skupien P. & Thomson S.N. 2018: The Žermanice sill: new insights into the mineralogy, petrology, age, and origin of the teschenite association rocks in the Western Carpathians, Czech Republic. *Int. J. Earth Sci.* 107, 7, 2553–2574.
- McDonough W.F. & Sun S.-S. 1995: The composition of the Earth. *Chem. Geol.* 120, 223–253.
- Miranda R., Valadares V., Terrinha P., Mata J., Azevedo M.D.R., Gaspar M., Kullberg J.C. & Ribeiro C. 2009: Age constraints on the Late Cretaceous alkaline magmatism on the West Iberian margin. *Cretaceous Res.* 30, 575–586.
- Narebski W. 1990: Early rift stage in the evolution of western part of the Carpathians: geochemical evidence from limburgite and teschenite rock series. *Geol. Carpath.* 41, 521–528.
- Nebel O., Arculus R.J., van Westrenen W., Woodhead J.D., Jenner F.E., Nebel-Jacobsen Y.J., Wille M. & Eggins S.M. 2013: Coupled Hf-Nd-Pb isotope co-variations of HIMU oceanic island basalts from Mangaia, Cook-Austral Islands, suggest an Archean source component in the mantle transition zone. *Geochim. Cosmochim. Acta* 112, 87–101.
- Nemčok M., Marko F., Kováč M. & Fodor L. 1989: Neogene tectonics and paleostress changes in the Czechoslovakian part of the Vienna Basin. *Jahrb. Geol. Bundesanst.* 132, 443–458.
- Nemčok M., Nemčok J., Wojtaszek M., Ludhova L., Oszczypko N., Sercombe W.J., Cieszkowski M., Paul Z., Coward M.P. & Ślączka A. 2001: Reconstruction of Cretaceous rifts incorporated in the outer west Carpathian wedge by balancing. *Mar. Petrol. Geol.* 18, 39–64.
- Oszczypko N. 2006: Late Jurassic–Miocene evolution of the Outer Carpathian fold-and-thrust belt and its foredeep basin (Western Carpathians, Poland). *Geol. Quarterly* 50, 169–194.
- Oszczypko N., Salata, D. & Krobicki M. 2012: Early Cretaceous intra-plate volcanism in the Pieniny Klippen Belt — a case study of the Velykyi Kamenets/Vilkhivchyk (Ukraine) and Biała Woda (Poland) sections. *Geol. Quarterly* 56, 629–648.
- Paton C., Hellstrom J., Paul B., Woodhead J. & Hergt J. 2011: Iolite: Freeware for the visualisation and processing of mass spectrometric data. *J. Anal. Atom. Spectrom.* 26, 2508.
- Pearce J.A. 1996: A user's guide to basalt discrimination diagrams. Trace element geochemistry of volcanic rocks: applications for massive sulphide exploration. *Geol. Assoc. Canada, Short Course Notes* 12, 79–113.
- Pearce J.A. 2008: Geochemical fingerprinting of oceanic basalts with applications to ophiolite classification and the search for Archean oceanic crust. *Lithos* 100, 14–48.
- Pedersen R.B., Dunning G.R. & Robins B. 1989: U–Pb ages of nepheline syenite pegmatites from the Seiland Magmatic Province, N Norway, In: Gayer, R.A. (Ed.), *The Caledonide Geology of Scandinavia*. *Springer Netherlands*, Dordrecht, 3–8.

- Piromallo C., Vincent A.P., Yuen D.A. & Morelli A. 2001: Dynamics of the transition zone under Europe inferred from wavelet cross-spectra of seismic tomography. *Phys. Earth Planet. Inter.* 125, 125–139.
- Rock N.M.S. 1982: The Late Cretaceous alkaline igneous province in the Iberian Peninsula, and its tectonic significance. *Lithos* 15, 111–131.
- Rögl F. 1996: Stratigraphic correlation of Paratethys Oligocene and Miocene. *Mitt. Gesell. Geol. Bergbau. Österreich* 41, 65–73.
- Rosenbusch H. 1887: Mikroskopische Physiographie der Mineralien und Gesteine. Vol. II. Massige Gesteine., 2nd ed. *Schweizerbart*, Stuttgart, 1–596.
- Rossy M., Azambre B. & Albarède F. 1992: REE and Sr/Nd isotope geochemistry of the alkaline magmatism from the Cretaceous North Pyrenean Rift Zone (France-Spain). *Chem. Geol.* 97, 33–46.
- Russell W.A., Papanastassiou D.A. & Tombrello T.A. 1978: Ca isotope fractionation on the Earth and other solar system materials. *Geochim. Cosmochim. Acta* 42, 1075–1090.
- Salter V.J.M. & White W.M. 1998: Hf isotope constraints on mantle evolution. *Chem. Geol.* 145, 447–460.
- Sandulescu M. 1988: Cenozoic tectonic history of the Carpathians. In: Royden L.H. & Horvath F. (Ed.): The Pannonian Basin – A Study in Basin Evolution. *AAPG Memoir*, 17–25.
- Sato H., Tchoua F. & Kusakabe M. 1991: Olivine phenocrysts in some Cameroonian basalts — implications for primary magma composition. *Mineral. Petrol.* 44, 253–269.
- Scherer E., Münker C. & Mezger K. 2001: Calibration of the lutetium–hafnium clock. *Science* 293, 683–687.
- Seghedi I., Downes H., Szakács A., Mason P.R.D., Thirlwall M.F., Emilian R., Pécskay Z., Márton E. & Panaiotu C. 2004a: Neogene–Quaternary magmatism and geodynamics in the Carpathian–Pannonian region: a synthesis. *Lithos* 72, 117–146.
- Seghedi I., Downes H., Vaselli O., Szakács A., Balogh K. & Pécskay Z. 2004b: Post-collisional Tertiary–Quaternary mafic alkalic magmatism in the Carpathian-Pannonian region: a review. *Tectonophysics* 393, 43–62.
- Simkin T. & Smith J.V. 1970: Minor-element distribution in olivine. *J. Geol.* 78, 304–325.
- Ślączka A., Oszczypko N., Malata E. & Cieszkowski M. 1999: An early history of the Outer Carpathian basin. *Geol. Carpath.* 50, 170–172.
- Stomka T. 1986: Statistical approach to study of flysch sedimentation – Kimmeridgian–Hauterivian Cieszyn beds, Polish Outer Carpathians. *Ann. Soc. Geol. Pol.* 56, 277–336.
- Smulikowski K. 1929: Materials on knowledge of magmatic rocks from Teschen region in Silesia. *Arch. Tow. Nauk. we Lwowie* 1, 1–122 (in Polish).
- Smulikowski K. 1980: Remarks on teschenite magmatic province (in Polish). *Ann. Soc. Geol. Pol.* L-1, 41–54.
- Sperner B., Ratschbacher L. & Nemčok M. 2002: Interplay between subduction retreat and lateral extrusion: Tectonics of the Western Carpathians. *Tectonics* 21, 1051.
- Spišiak J. & Balogh K. 2002: Mesozoic alkali lamprophyres in Variscan granitoids of the Malé Karpaty and Nízké Tatry Mountains — geochronology and geochemistry. *Geol. Carpath.* 53, 295–301.
- Spišiak J., Plašienka D., Bučová J., Mikuš T. & Uher P. 2011: Petrology and palaeotectonic setting of Cretaceous alkaline basaltic volcanism in the Pieniny Klippen Belt (Western Carpathians, Slovakia). *Geol. Quarterly* 55, 27–48.
- Stacey J.S. & Kramers J.D. 1975: Approximation of terrestrial lead isotope evolution by a two-stage model. *Earth Planet. Sci. Lett.* 26, 207–221.
- Sun S.-S. & McDonough W.F. 1989: Chemical and isotopic systematics of oceanic basalts: implications for mantle composition and processes. In: Saunders A.D. & Norry M.J. (Eds.): Magmatism in the Ocean Basins. *Geol. Soc. London, Spec. Pub.* 42, 313–345.
- Švábenická L., Bubík M., Krejčí O. & Stráník Z. 1997: Stratigraphy of Cretaceous Sediments of the Magura Group of Nappes in Moravia (Czech Republic). *Geol. Carpath.* 48, 179–191.
- Szopa K., Włodyka R. & Chew D. 2014: LA-ICP-MS U–Pb apatite dating of Lower Cretaceous rocks from teschenite-picrite association in the Silesian Unit (southern Poland). *Geol. Carpath.* 65, 273–284.
- Tindle A.G. & Webb P.C. 1990: Formula Unit Calculations — with optional calculated Li₂O, 2. Li₂O and H₂O calculations. *European J. Mineral.* 2, 595–610.
- Tschermak G. 1866: Felsarten von ungewöhnlicher Zusammensetzung in den Umgebung von Teschen und Neutitschein. *Sitz.-Ber. Akad. Wiss. (Wien)* 53, 260–287.
- Ulrych J., Pivec E., Žák K., Bendl J. & Bosák P. 1993: Alkaline and ultramafic carbonate lamprophyres in Central Bohemian carboniferous basins, Czech Republic. *Mineral. Petrol.* 48, 65–81.
- Ulrych J., Dostál J., Adamovič J., Jelínek E., Špaček P., Hegner E. & Balogh K. 2011: Recurrent Cenozoic volcanic activity in the Bohemian Massif (Czech Republic). *Lithos* 123, 133–144.
- Vervoort J.D., Plank T. & Prytulak J. 2011: The Hf–Nd isotopic composition of marine sediments. *Geochim. Cosmochim. Acta* 75, 5903–5926.
- Villa I.M. 1998: Isotopic closure. *Terra Nova* 10, 42–47.
- Villa I.M., De Bièvre P., Holden N.E. & Renne P.R. 2015: IUPAC–IUGS recommendation on the half life of ⁸⁷Rb. *Geochim. Cosmochim. Acta* 164, 382–385.
- Willbold M. & Stracke A. 2006: Trace element composition of mantle end-members: implications for recycling of oceanic and upper and lower continental crust. *Geochem. Geophys. Geosys.* 7, 1–30.
- Wilson M. & Bianchini G. 1999: Tertiary–Quaternary magmatism within the Mediterranean and surrounding regions. In: Durand B., Jolivet L., Horváth F. & Séranne M. (Eds.): Tertiary–Quaternary magmatism within the Mediterranean and surrounding regions. *Geol. Soc. London, Spec. Publ.* 156, 141–168.
- Wilson M. & Downes H. 1991: Tertiary–Quaternary Extension-Related Alkaline Magmatism in Western and Central Europe. *J. Petrol.* 32, 811–849.
- Wilson M. & Downes H. 2006: Tertiary–Quaternary intra-plate magmatism in Europe and its relationship to mantle dynamics. In: Gee D.G. & Stephenson R.A. (Eds.): European Lithosphere Dynamics. *Geol. Soc. London, Memoires* 32, 147–166.
- Włodyka R. 2010: The evolution of mineral composition of the Cieszyn magma province rocks. *Wydawnictwo Uniwersytetu Śląskiego*, Katowice, 1–232 (in Polish).
- Woodhead J.D. 1996: Extreme HIMU in an oceanic setting: the geochemistry of Mangaia Island (Polynesia), and temporal evolution of the Cook–Austral hotspot. *J. Volcan. Geotherm. Res.* 72, 1–19.
- Żytko K., Gucik S., Rylko W., Oszczypko N., Zajac R., Garlicka I., Nemčok J., Eliáš M., Menčík E. & Stráník Z. 1989: Map of the tectonic elements of the Western Outer Carpathians and their Foreland. In: Poprawa D. & Nemčok J. (Eds.): Geological Atlas of the Western Outer Carpathians and Their Foreland. *Państwowy Instytut Geologiczny*, Warszawa.

Supplement

Table S1: Electron microprobe analyses of the selected phenocrysts.

Representative pyroxene compositions from Teschenite Association Rocks samples

Rock type: Mineral: Sample:	Picrite		Picroteschenite									
	Di CPR1-1	Di CPR1-1	Di CS4-2.	Di CS4-2.	Di CS4-3	Di CS4-3	Di CSTa2-2	Di CSTa2-2	Di CR6-2	Di CR6-2	Di CR6-4	Di CR6-4
	2	8	2	3	4	5	8	11	5	9	4	5
	uniform	uniform	bright rim	dark core	bright zone	dark zone	dark core	very bright rim	dark zone	bright zone	bright core	dark zone
SiO ₂	46.79	47.86	43.59	50.37	47.96	49.86	47.17	48.87	48.52	43.70	43.31	46.59
TiO ₂	2.18	2.13	3.39	1.25	1.94	1.46	2.61	1.34	2.08	3.25	3.97	2.70
Al ₂ O ₃	6.62	5.97	8.63	3.36	5.20	3.68	5.73	2.28	4.48	7.86	8.30	6.21
Cr ₂ O ₃	0.76	0.77	0.01	0.39	0.04	0.21	0.47	0.07	0.01	0.00	0.00	0.12
Fe ₂ O ₃	4.06	3.27	5.62	3.26	4.60	3.29	3.89	4.34	2.95	5.67	5.67	4.15
FeO	1.80	1.93	2.76	2.31	2.85	2.66	1.96	11.20	3.65	3.28	2.33	1.94
MnO	0.04	0.08	0.11	0.08	0.14	0.11	0.00	0.53	0.17	0.09	0.04	0.00
MgO	13.38	13.88	11.13	15.02	13.53	14.67	13.80	8.05	13.63	11.07	11.52	13.27
CaO	24.10	24.17	23.66	23.93	23.71	23.90	23.97	22.43	23.78	23.55	23.97	24.21
Na ₂ O	0.29	0.30	0.45	0.33	0.34	0.30	0.32	1.04	0.28	0.41	0.37	0.33
K ₂ O	0.00	0.01	0.02	0.00	0.01	0.00	0.00	0.00	0.00	0.00	0.01	0.00
Total	100.02	100.38	99.37	100.30	100.32	100.14	99.92	100.14	99.56	98.88	99.49	99.52
No. oxyg.	6	6	6	6	6	6	6	6	6	6	6	6
Si	1.737	1.765	1.648	1.854	1.780	1.841	1.752	1.884	1.812	1.664	1.636	1.739
Ti	0.061	0.059	0.096	0.035	0.054	0.041	0.073	0.039	0.058	0.093	0.113	0.076
Al	0.290	0.260	0.385	0.146	0.227	0.160	0.251	0.104	0.197	0.353	0.369	0.273
Cr	0.022	0.022	0.000	0.011	0.001	0.006	0.014	0.002	0.000	0.000	0.000	0.004
Fe ³⁺	0.113	0.091	0.160	0.090	0.129	0.091	0.109	0.126	0.083	0.162	0.161	0.117
Fe ²⁺	0.056	0.060	0.087	0.071	0.088	0.082	0.061	0.361	0.114	0.104	0.073	0.060
Mn	0.001	0.002	0.004	0.002	0.004	0.003	0.000	0.017	0.005	0.003	0.001	0.000
Mg	0.740	0.763	0.627	0.824	0.748	0.808	0.764	0.463	0.759	0.629	0.649	0.739
Ca	0.959	0.955	0.959	0.944	0.943	0.946	0.954	0.927	0.951	0.961	0.970	0.968
Na	0.021	0.021	0.033	0.024	0.024	0.021	0.023	0.078	0.020	0.030	0.027	0.024
K	0.000	0.000	0.001	0.000	0.000	0.000	0.000	0.000	0.000	0.000	0.000	0.000
Total	4.000	4.000	4.000	4.000	4.000	4.000	4.000	4.000	4.000	4.000	4.000	4.000
Mg no.	0.930	0.928	0.878	0.921	0.894	0.908	0.926	0.562	0.869	0.857	0.898	0.924

All analyses by electron microprobe; Di - diopside, He - hedenbergite, Aug - augite

Table S1 (continued): Electron microprobe analyses of the selected phenocrysts.

Representative pyroxene compositions from Teschenite Association Rocks samples

Rock type: Mineral: Sample:	Teschenite												Syenite				
	Di CBL1-2 21	Di CBL1-2 22	Di CRE3-1 12	Di CRE3-1 19	He CRE3-2 32	Di CRE3-3 33	Di CRE3-3 7	He CRE3-3 8	Di CRE3-4 7	Di CRE3-4 11	He CRE3-4 12	Di CZI1-1 9	Di CZI1-1 10	Aug CZI1-1 13	Aug CZI1-4 1		
	uniform	uniform	dark zone	bright zone	bright rim	dark core	brighter zone	very bright rim	dark core	brighter zone 2	very bright rim	uniform	uniform	uniform	uniform	uniform	
	SiO ₂	44.46	41.97	49.36	44.57	46.15	46.14	47.56	46.31	48.93	49.9	46.7	49.45	48.64	51.23	50.44	
TiO ₂	3.31	4.57	1.85	3.54	1.82	2.62	2.12	1.46	1.96	1.39	1.74	1.81	2.13	0.85	0.99		
Al ₂ O ₃	7.86	9.44	4.06	6.99	2.75	5.71	4.79	2.11	3.85	3.09	3.01	3.46	4.08	1.95	2.39		
Cr ₂ O ₃	0.00	0.03	0.00	0.01	0.00	0.01	0	0	0.01	0.01	0	0	0.01	0	0		
Fe ₂ O ₃	5.27	5.80	3.42	5.08	6.33	4.22	3.31	4.68	3.38	2.13	4.49	2.78	3.28	1.37	2.54		
FeO	2.50	2.94	3.62	3.79	17.74	6.92	6.34	19.77	3.88	7.14	15.33	5.97	5.92	9.82	7.83		
MnO	0.10	0.08	0.17	0.09	0.94	0.33	0.27	0.99	0.11	0.26	0.86	0.17	0.2	0.36	0.37		
MgO	11.88	10.61	13.72	11.50	2.22	9.94	11	1.68	13.67	11.95	4.53	13.67	13.45	13.76	14.22		
CaO	23.86	23.70	23.47	23.04	19.72	22.95	23.08	19.94	23.28	23.26	20.84	22.03	21.81	20.05	20.35		
Na ₂ O	0.38	0.43	0.51	0.55	1.92	0.68	0.63	1.57	0.45	0.52	1.38	0.43	0.44	0.35	0.34		
K ₂ O	0.01	0.00	0.00	0.01	0.00	0	0.02	0.03	0	0	0.01	0.01	0	0	0		
Total	99.63	99.57	100.18	99.17	99.59	99.52	99.12	98.54	99.52	99.65	98.89	99.78	99.96	99.74	99.47		
No. oxyg.	6	6	6	6	6	6	6	6	6	6	6	6	6	6	6		
Si	1.672	1.591	1.830	1.691	1.859	1.761	1.808	1.895	1.829	1.881	1.863	1.850	1.820	1.926	1.896		
Ti	0.094	0.130	0.052	0.101	0.055	0.075	0.061	0.045	0.055	0.039	0.052	0.051	0.060	0.024	0.028		
Al	0.348	0.422	0.177	0.312	0.131	0.257	0.215	0.102	0.170	0.137	0.142	0.153	0.180	0.086	0.106		
Cr	0.000	0.001	0.000	0.000	0.000	0.000	0.000	0.000	0.000	0.000	0.000	0.000	0.000	0.000	0.000		
Fe ³⁺	0.149	0.165	0.095	0.145	0.192	0.121	0.095	0.144	0.095	0.060	0.135	0.078	0.092	0.039	0.072		
Fe ²⁺	0.079	0.093	0.112	0.120	0.598	0.221	0.202	0.677	0.121	0.225	0.512	0.187	0.185	0.309	0.246		
Mn	0.003	0.003	0.005	0.003	0.032	0.011	0.009	0.034	0.003	0.008	0.029	0.005	0.006	0.011	0.012		
Mg	0.666	0.600	0.758	0.650	0.133	0.565	0.624	0.102	0.762	0.671	0.269	0.762	0.750	0.771	0.797		
Ca	0.961	0.963	0.932	0.936	0.851	0.938	0.940	0.874	0.932	0.939	0.891	0.883	0.874	0.808	0.819		
Na	0.028	0.032	0.037	0.040	0.150	0.050	0.046	0.125	0.033	0.038	0.107	0.031	0.032	0.026	0.025		
K	0.000	0.000	0.000	0.000	0.000	0.000	0.001	0.002	0.000	0.000	0.001	0.000	0.000	0.000	0.000		
Total	4.000	4.000	4.000	4.000	4.000	4.000	4.000	4.000	4.000	4.000	4.000	4.000	4.000	4.000	4.000		
Mg no.	0.894	0.865	0.871	0.844	0.182	0.719	0.756	0.132	0.863	0.749	0.345	0.803	0.802	0.714	0.764		

All analyses by electron microprobe; Di - diopside, He - hedenbergite, Aug - augite

Table S1 (continued): Electron microprobe analyses of the selected phenocrysts.

Representative amphibole compositions from Teschenite Association Rocks samples

Group:	OH,F,Cl	OH,F,Cl	oxo	oxo	OH,F,Cl	OH,F,Cl	OH,F,Cl	OH,F,Cl	OH,F,Cl	oxo
Subgroup:	Ca	Ca	B = Ca	B = Ca	Ca	Ca	Ca	Ca	Ca	B = Ca
Species:	Ti-par	Ti-rich par	ferri-kaer	ferro-ferri-kaer	Ti-ferro-Par	Ti-par	Ti-Par	Ti-par	K-hast	ferro-ferri-kaer
Sample:	CPR-1-3	CPR-1-3	CRE3-1	CRE3-3	CS4-1	CS4-	CSTa2-1	CSTa2-1	CBL1-2	CBL1-2
	15	16	6	1	1	7	12	21	3	4
	uniform	uniform	uniform	overgrowth on px	uniform	rim on px	uniform	uniform	bright rim	dark core
SiO ₂	40.49	41.07	39.08	39.13	37.73	37.51	40.10	39.15	35.21	35.25
TiO ₂	3.86	3.63	5.08	4.65	2.91	3.55	4.20	4.20	0.64	4.38
ZrO ₂	0.02	0.02	0.04	0.05	0.13	0.06	0.06	0.00	0.03	0.08
Al ₂ O ₃	13.95	13.37	12.39	11.91	14.30	15.66	13.17	13.75	14.58	15.95
Cr ₂ O ₃	0.22	0.12	0.00	0.01	0.00	0.00	0.05	0.04	0.02	0.01
MnO	0.10	0.10	0.33	0.47	0.45	0.34	0.18	0.21	0.70	0.41
Mn ₂ O ₃	0.00	0.00	0.00	0.00	0.00	0.00	0.00	0.00	0.00	0.00
FeO	8.22	8.24	10.66	13.34	17.35	15.13	12.03	12.24	25.89	13.16
Fe ₂ O ₃	0.00	0.00	7.39	6.51	1.65	0.89	0.00	0.08	5.04	8.08
NiO	0.06	0.08	0.07	0.00	0.02	0.02	0.00	0.09	0.00	0.02
MgO	14.33	14.61	8.62	7.25	7.79	9.15	12.11	12.00	0.24	5.22
CaO	12.43	12.42	11.82	11.46	11.59	12.01	12.12	12.19	10.52	11.89
Na ₂ O	2.66	2.53	2.66	2.68	2.26	2.33	2.60	2.53	1.86	1.92
K ₂ O	1.39	1.43	1.11	1.29	1.53	1.46	1.37	1.38	2.66	1.84
H ₂ O ⁺	2.05	2.02	0.76	0.84	1.90	1.96	1.96	2.01	1.81	0.81
F	0.00	0.06	0.12	0.10	0.11	0.03	0.11	0.00	0.06	0.24
Cl	0.00	0.00	0.00	0.00	0.00	0.00	0.00	0.00	0.00	0.00
O=F,Cl (calc)	0.00	-0.03	-0.05	-0.04	-0.05	-0.01	-0.05	0.00	-0.03	-0.10
Total	99.78	99.67	100.08	99.65	99.68	100.09	100.01	99.87	99.22	99.16
No. oxyg.	22	22	22	22	22	22	22	22	22	22
Si	5.936	6.021	5.979	6.069	5.815	5.685	5.967	5.853	5.773	5.548
Al	2.064	1.979	2.021	1.931	2.185	2.315	2.033	2.147	2.227	2.452
Ti	0.000	0.000	0.000	0.000	0.000	0.000	0.000	0.000	0.000	0.000
Fe ³⁺	0.000	0.000	0.000	0.000	0.000	0.000	0.000	0.000	0.000	0.000
[T]	8.000	8.000	8.000	8.000	8.000	8.000	8.000	8.000	8.000	8.000
Ti	0.426	0.400	0.585	0.543	0.337	0.405	0.470	0.472	0.079	0.519
Zr	0.001	0.001	0.003	0.004	0.010	0.004	0.004	0.000	0.002	0.006
Al	0.346	0.331	0.214	0.246	0.413	0.482	0.277	0.276	0.591	0.507
Cr	0.026	0.014	0.000	0.001	0.000	0.000	0.006	0.005	0.003	0.001
Mn ³⁺	0.000	0.000	0.000	0.000	0.000	0.000	0.000	0.000	0.000	0.000
Fe ³⁺	0.000	0.000	0.851	0.759	0.193	0.102	0.000	0.009	0.623	0.957
Ni	0.007	0.009	0.009	0.000	0.002	0.002	0.000	0.011	0.000	0.003
Mn ²⁺	0.012	0.012	0.009	0.039	0.019	0.020	0.023	0.022	0.095	0.051
Fe ²⁺	1.008	1.010	1.363	1.731	2.236	1.917	1.497	1.531	3.548	1.732
Mg	3.132	3.193	1.966	1.676	1.790	2.067	2.686	2.675	0.059	1.225
[C]	4.958	4.970	5.000	4.999	5.000	4.999	4.963	5.001	5.000	5.001
Mn ²⁺	0.000	0.000	0.034	0.023	0.040	0.023	0.000	0.005	0.002	0.004
Fe ²⁺	0.000	0.000	0.000	0.000	0.000	0.000	0.000	0.000	0.000	0.000
Mg	0.000	0.000	0.000	0.000	0.000	0.000	0.000	0.000	0.000	0.000
Ca	1.953	1.951	1.938	1.904	1.914	1.950	1.932	1.953	1.848	1.996
Na	0.047	0.049	0.029	0.073	0.046	0.027	0.068	0.042	0.150	0.000
[B]	2.000	2.000	2.001	2.000	2.000	2.000	2.000	2.000	2.000	2.000
Ca	0.000	0.000	0.000	0.000	0.000	0.000	0.000	0.000	0.000	0.000
Na	0.709	0.670	0.761	0.733	0.629	0.658	0.682	0.691	0.441	0.586
K	0.260	0.267	0.217	0.255	0.301	0.282	0.260	0.263	0.556	0.369
[A]	0.969	0.937	0.978	0.988	0.930	0.940	0.942	0.954	0.997	0.964
OH	2.000	1.972	0.774	0.867	1.946	1.986	1.948	2.000	1.969	0.844
F	0.000	0.028	0.058	0.049	0.054	0.014	0.052	0.000	0.031	0.119
Cl	0.000	0.000	0.000	0.000	0.000	0.000	0.000	0.000	0.000	0.000
O	0.000	0.000	1.168	1.084	0.000	0.000	0.000	0.000	0.000	1.036
[W]	2.000	2.000	2.000	2.000	2.000	2.000	2.000	2.000	2.000	1.999
Total	15.927	15.907	15.979	15.987	15.930	15.939	15.905	15.955	15.997	15.965

All analyses by electron microprobe; Amphibole formula calculated after Locock (2014); Ti-par – Ti-pargasite; Ti-rich par – Ti rich pargasite; ferri-Kaer – ferri kaersutite; K-hast – K-hastingsite; ferro-ferri-kaer – ferro-ferri-kaersutite

Table S1 (continued): Electron microprobe analyses of the selected phenocrysts.

Representative mica compositions from Teschenite Association Rocks samples

Rock:	Pierite						Picroteschenite								
	Mineral:	Bt	Bt	Bt	Phl	Phl	Phl	Bt							
		CPR1-1	CPR1-1	CPR1-1	CPR-1-4.	CPR-1-4.	CPR-1-4.	CSTa-2-3							
	1	2	13	4	6	7	2	3	4	5	6	7	8	9	
SiO ₂	37.24	36.87	36.56	37.39	36.54	39.35	36.21	37.05	35.88	37.20	36.72	36.86	36.86	37.00	
TiO ₂	6.07	6.18	5.01	3.61	5.38	3.92	6.02	6.15	6.55	6.14	6.02	5.63	5.96	5.80	
Al ₂ O ₃	17.23	17.19	16.68	16.16	16.97	12.45	16.69	16.80	16.39	16.97	16.56	16.66	16.83	16.86	
FeO	7.67	7.42	9.34	7.77	7.80	8.75	11.03	10.21	10.19	10.02	11.15	12.93	11.69	11.88	
MnO	0.12	0.12	0.04	0.07	0.07	0.07	0.12	0.07	0.07	0.12	0.10	0.20	0.06	0.09	
MgO	18.16	18.29	17.79	19.75	18.60	23.68	15.72	16.57	15.50	16.83	16.02	15.17	15.94	15.97	
CaO	0.00	0.00	0.10	0.25	0.15	0.13	0.00	0.00	0.00	0.00	0.00	0.00	0.00	0.00	
Na ₂ O	0.86	0.86	1.59	1.59	1.06	0.62	0.69	0.73	0.69	0.72	0.70	0.66	0.76	0.67	
K ₂ O	8.44	8.17	7.32	7.50	8.09	4.90	8.27	8.33	8.18	8.23	8.37	8.55	8.19	8.43	
BaO	0.65	0.77	0.39	0.24	0.80	0.50	0.47	0.57	0.76	0.69	0.56	0.50	0.52	0.43	
F	0.00	0.09	0.21	0.00	0.11	0.00	0.18	0.03	0.25	0.07	0.13	0.00	0.11	0.02	
Cl	0.00	0.00	0.00	0.00	0.00	0.00	0.00	0.00	0.00	0.00	0.00	0.00	0.00	0.00	
Cr ₂ O ₃	0.11	0.14	0.11	0.05	0.04	0.00	0.01	0.03	0.00	0.00	0.00	0.00	0.05	0.00	
H ₂ O*	4.20	4.14	4.02	4.13	4.10	4.18	3.99	4.14	3.92	4.14	4.06	4.13	4.09	4.15	
O=F,Cl	0.00	0.04	0.09	0.00	0.05	0.00	0.08	0.01	0.11	0.03	0.05	0.00	0.05	0.01	
Total	100.75	100.20	99.07	98.51	99.66	98.55	99.32	100.67	98.27	101.10	100.34	101.29	101.01	101.29	
No. oxyg.	22	22	22	22	22	22	22	22	22	22	22	22	22	22	
Si	5.311	5.284	5.323	5.429	5.282	5.645	5.315	5.340	5.317	5.334	5.339	5.352	5.326	5.336	
Al iv	2.689	2.716	2.677	2.571	2.718	2.105	2.685	2.660	2.683	2.666	2.661	2.648	2.674	2.664	
[T]	8.000	8.000	8.000	8.000	8.000	7.751	8.000	8.000	8.000	8.000	8.000	8.000	8.000	8.000	
Al vi	0.207	0.188	0.185	0.194	0.173	0.000	0.202	0.195	0.180	0.202	0.178	0.203	0.193	0.202	
Ti	0.651	0.666	0.549	0.394	0.585	0.423	0.665	0.667	0.730	0.662	0.658	0.615	0.648	0.629	
Cr	0.012	0.016	0.013	0.006	0.005	0.000	0.001	0.003	0.000	0.000	0.000	0.000	0.006	0.000	
Fe	0.915	0.889	1.137	0.943	0.943	1.050	1.354	1.231	1.263	1.202	1.356	1.570	1.413	1.433	
Mn	0.014	0.015	0.005	0.009	0.009	0.009	0.015	0.009	0.009	0.015	0.012	0.025	0.007	0.011	
Mg	3.861	3.907	3.861	4.275	4.008	5.064	3.440	3.560	3.424	3.597	3.472	3.283	3.433	3.433	
[M]	5.661	5.681	5.749	5.821	5.722	6.546	5.677	5.664	5.605	5.678	5.676	5.695	5.699	5.708	
Ca	0.000	0.000	0.016	0.039	0.023	0.020	0.000	0.000	0.000	0.000	0.000	0.000	0.000	0.000	
Na	0.238	0.239	0.449	0.448	0.297	0.172	0.196	0.204	0.198	0.200	0.197	0.186	0.213	0.187	
K	1.535	1.493	1.359	1.389	1.492	0.897	1.548	1.531	1.546	1.505	1.552	1.583	1.509	1.551	
Ba	0.036	0.043	0.022	0.014	0.045	0.028	0.027	0.032	0.044	0.039	0.032	0.028	0.029	0.024	
[A]	1.809	1.776	1.846	1.889	1.857	1.117	1.772	1.768	1.789	1.744	1.782	1.798	1.752	1.762	
Total	15.470	15.456	15.595	15.710	15.580	15.414	15.449	15.432	15.394	15.422	15.458	15.493	15.451	15.471	
OH*	4.000	3.959	3.903	4.000	3.950	4.000	3.916	3.986	3.883	3.968	3.940	4.000	3.950	3.991	
F	0.000	0.041	0.097	0.000	0.050	0.000	0.084	0.014	0.117	0.032	0.060	0.000	0.050	0.009	
Cl	0.000	0.000	0.000	0.000	0.000	0.000	0.000	0.000	0.000	0.000	0.000	0.000	0.000	0.000	
Al total	2.896	2.904	2.862	2.766	2.891	2.105	2.888	2.854	2.863	2.868	2.838	2.851	2.866	2.866	
Fe/Fe+Mg	0.192	0.185	0.228	0.181	0.190	0.172	0.282	0.257	0.269	0.250	0.281	0.323	0.292	0.294	

All analyses by electron microprobe; H₂O calculations after Tindle & Webb (1990); Bt - biotite, Phl - phlogopite

Table S1 (continued): Electron microprobe analyses of the selected phenocrysts.

Representative olivine compositions from Teschenite Association Rocks samples

Rock type: Mineral: Formula	Picrite							
	Ol CPR1-2 5	Ol CPR1-2 6	Ol CPR1-3 9	Ol CPR1-3 10	Ol CPR1-3 11	Ol CPR1-3 12	Ol CPR1-4 1	Ol CPR1-4 2
	44.13	44.25	44.09	44.65	44.05	42.95	44.62	44.91
MgO	0.48	0.46	0.44	0.33	0.41	0.48	0.42	0.41
CaO	0.30	0.25	0.24	0.25	0.29	0.32	0.32	0.19
MnO	15.61	15.21	14.63	13.95	14.75	16.59	14.55	14.37
NiO	0.07	0.19	0.16	0.16	0.09	0.15	0.11	0.19
Al ₂ O ₃	0.03	0.04	0.03	0.04	0.03	0.01	0.02	0.03
Cr ₂ O ₃	0.01	0.02	0.01	0.02	0.03	0.01	0.02	0.03
SiO ₂	40.10	40.30	40.00	40.62	39.98	39.92	40.37	40.67
TiO ₂	0.03	0.02	0.02	0.01	0.01	0.02	0.01	0.01
Total	100.77	100.75	99.62	100.04	99.64	100.44	100.45	100.81
No. oxygens	4	4	4	4	4	4	4	4
Mg	1.645	1.646	1.655	1.661	1.654	1.614	1.660	1.662
Ca	0.013	0.012	0.012	0.009	0.011	0.013	0.011	0.011
Mn	0.006	0.005	0.005	0.005	0.006	0.007	0.007	0.004
Fe ²⁺ (tot)	0.326	0.317	0.308	0.291	0.311	0.350	0.304	0.298
Ni	0.001	0.004	0.003	0.003	0.002	0.003	0.002	0.004
Al	0.001	0.001	0.001	0.001	0.001	0.000	0.001	0.001
Cr	0.000	0.000	0.000	0.000	0.001	0.000	0.000	0.001
Si	1.003	1.006	1.007	1.014	1.007	1.006	1.007	1.009
Ti	0.000	0.000	0.000	0.000	0.000	0.000	0.000	0.000
Total cations	2.996	2.993	2.992	2.985	2.992	2.993	2.992	2.990
Fo%	83.210	83.640	84.100	84.870	83.920	81.890	84.220	84.620
Mg/Mg+Fe	0.835	0.839	0.843	0.851	0.842	0.822	0.845	0.848

Ol - olivine

Table S2: Summary of laser ablation ICP-MS U–Pb titanite dating results.

Isotope ratios							Ages (Ma)						
$^{207}\text{Pb}/^{235}\text{U}$	$\pm 2\text{SE}$	$^{206}\text{Pb}/^{238}\text{U}$	$\pm 2\text{SE}$	$^{238}\text{U}/^{206}\text{Pb}$	$\pm 2\text{SE}$	$^{207}\text{Pb}/^{206}\text{Pb}$	$\pm 2\text{SE}$	$^{206}\text{Pb}/^{238}\text{U}$ age	$\pm 2\text{SE}$	$^{207}\text{Pb}/^{235}\text{U}$ age	$\pm 2\text{SE}$	$^{207}\text{Pb-corr. Age}$	$\pm 2\text{SE}$
Sample CP1-11													
0.520	0.065	0.0219	0.0013	45.66	2.71	0.170	0.023	139.7	8.4	405	44	117.5	9.3
1.050	0.180	0.0255	0.0022	39.22	3.38	0.331	0.063	162.0	14.0	686	90	114.0	21.0
1.000	0.120	0.0256	0.0017	39.06	2.59	0.309	0.040	163.0	11.0	661	61	114.0	12.0
0.548	0.076	0.0215	0.0014	46.51	3.03	0.190	0.029	136.8	9.1	410	49	114.0	11.0
1.161	0.088	0.0271	0.0012	36.90	1.63	0.315	0.025	172.0	7.4	759	40	115.7	9.6
0.431	0.057	0.0210	0.0010	47.53	2.26	0.153	0.021	134.1	6.3	354	41	117.8	8.3
0.356	0.046	0.0217	0.0011	46.08	2.34	0.126	0.017	138.0	7.2	298	34	125.6	8.0
0.432	0.081	0.0229	0.0021	43.67	4.00	0.141	0.031	146.0	14.0	347	59	129.0	14.0
0.430	0.110	0.0205	0.0018	48.78	4.28	0.146	0.037	131.0	11.0	330	78	114.0	14.0
0.447	0.072	0.0225	0.0015	44.44	2.96	0.160	0.028	143.4	9.3	346	50	128.0	12.0
0.484	0.079	0.0217	0.0014	46.08	2.97	0.186	0.036	139.3	9.3	365	51	120.0	12.0
0.759	0.090	0.0238	0.0014	42.02	2.47	0.256	0.033	151.4	8.9	546	52	116.0	11.0
0.416	0.052	0.0217	0.0010	46.15	2.13	0.143	0.020	138.1	6.3	334	38	123.5	8.0
0.405	0.060	0.0203	0.0013	49.26	3.15	0.148	0.023	129.5	8.2	321	42	113.9	9.2
0.439	0.070	0.0204	0.0013	49.02	3.12	0.164	0.028	130.3	8.5	338	48	112.9	9.7
0.396	0.072	0.0224	0.0015	44.64	2.99	0.137	0.027	142.6	9.1	315	52	128.0	11.0
0.476	0.074	0.0217	0.0013	46.08	2.76	0.175	0.032	138.0	8.2	368	51	119.7	9.4
0.570	0.130	0.0223	0.0015	44.84	3.02	0.185	0.038	142.0	9.6	417	73	118.5	9.8
0.308	0.037	0.0201	0.0010	49.70	2.40	0.113	0.015	128.3	6.1	266	29	118.0	6.9
0.372	0.082	0.0218	0.0018	45.87	3.79	0.133	0.031	139.0	12.0	298	60	123.0	12.0
0.400	0.100	0.0219	0.0019	45.66	3.96	0.137	0.035	140.0	12.0	306	71	125.0	13.0
0.506	0.085	0.0216	0.0013	46.30	2.79	0.175	0.029	137.8	8.0	375	54	117.0	9.6
0.429	0.062	0.0211	0.0014	47.39	3.14	0.158	0.026	134.5	9.0	337	44	117.0	11.0
1.310	0.100	0.0289	0.0014	34.60	1.68	0.359	0.038	183.4	9.0	827	45	119.0	13.0
0.511	0.081	0.0223	0.0014	44.84	2.82	0.182	0.031	142.0	8.8	380	53	121.0	10.0
0.373	0.050	0.0214	0.0011	46.73	2.40	0.134	0.019	136.5	7.1	308	38	122.7	8.2
0.640	0.100	0.0234	0.0015	42.74	2.74	0.205	0.035	149.1	9.5	467	63	120.0	13.0
1.280	0.140	0.0290	0.0015	34.48	1.78	0.305	0.033	184.0	9.7	798	59	128.0	12.0
0.446	0.065	0.0227	0.0013	44.05	2.52	0.153	0.025	144.5	8.3	349	43	126.8	9.9
0.422	0.056	0.0223	0.0012	44.84	2.41	0.145	0.021	142.0	7.5	342	41	125.7	9.1
0.985	0.082	0.0259	0.0013	38.61	1.94	0.286	0.025	164.8	7.9	678	44	118.8	9.3
1.590	0.150	0.0301	0.0019	33.22	2.10	0.422	0.050	191.0	12.0	928	61	110.0	15.0
0.630	0.100	0.0233	0.0015	42.92	2.76	0.206	0.030	148.5	9.4	447	58	116.4	9.5
0.351	0.029	0.0204	0.0006	49.02	1.35	0.123	0.010	130.2	3.6	301	21	118.6	4.0
Sample CR8-11													
0.530	0.150	0.0231	0.0026	43.29	4.87	0.198	0.060	147.0	17.0	430	110	121.0	20.0
0.330	0.052	0.0224	0.0014	44.64	2.79	0.120	0.022	142.4	8.7	280	41	131.0	9.8
0.416	0.057	0.0210	0.0014	47.62	3.17	0.156	0.023	133.5	9.0	342	43	116.3	9.9
0.334	0.054	0.0203	0.0013	49.26	3.15	0.131	0.024	129.4	8.2	270	40	117.3	9.4
0.328	0.057	0.0217	0.0014	46.08	2.97	0.122	0.022	138.0	8.9	268	42	126.3	10.0
0.316	0.046	0.0197	0.0011	50.76	2.83	0.119	0.019	125.5	6.9	267	36	114.4	7.9
0.482	0.083	0.0221	0.0016	45.25	3.28	0.178	0.035	140.5	10.0	376	57	122.0	13.0
0.368	0.067	0.0209	0.0015	47.85	3.43	0.137	0.025	133.3	9.6	293	49	120.0	11.0
0.350	0.063	0.0191	0.0013	52.36	3.56	0.134	0.024	121.6	8.5	282	47	108.2	9.3
0.397	0.067	0.0202	0.0013	49.50	3.19	0.158	0.030	128.5	8.4	315	49	114.0	10.0
0.368	0.062	0.0195	0.0014	51.28	3.68	0.147	0.026	124.1	9.0	296	45	110.0	10.0
0.285	0.053	0.0210	0.0015	47.62	3.40	0.116	0.025	133.9	9.3	233	39	125.0	11.0
0.358	0.060	0.0206	0.0014	48.54	3.30	0.138	0.026	131.3	8.9	286	43	118.6	10.0
0.323	0.047	0.0206	0.0010	48.52	2.35	0.122	0.018	131.5	6.4	267	36	121.0	7.7
0.301	0.051	0.0205	0.0011	48.90	2.63	0.109	0.019	130.4	6.7	252	39	120.5	7.4
0.292	0.048	0.0198	0.0011	50.51	2.81	0.111	0.018	126.2	6.9	242	36	117.5	8.1
0.399	0.064	0.0194	0.0012	51.55	3.19	0.155	0.027	123.9	7.6	312	46	107.4	9.2
0.341	0.060	0.0197	0.0015	50.76	3.87	0.148	0.030	125.4	9.2	277	45	114.0	11.0
0.357	0.059	0.0210	0.0016	47.62	3.63	0.134	0.028	133.6	10.0	284	43	123.0	11.0
0.374	0.054	0.0209	0.0015	47.85	3.43	0.154	0.027	133.2	9.5	313	42	119.0	11.0
0.301	0.056	0.0213	0.0014	46.95	3.09	0.117	0.024	135.6	8.8	243	42	125.7	10.0

Table S2 (continued): Summary of laser ablation ICP-MS U–Pb titanite dating results.

Isotope ratios							Ages (Ma)						
$^{207}\text{Pb}/^{235}\text{U}$	$\pm 2\text{SE}$	$^{206}\text{Pb}/^{238}\text{U}$	$\pm 2\text{SE}$	$^{238}\text{U}/^{206}\text{Pb}$	$\pm 2\text{SE}$	$^{207}\text{Pb}/^{206}\text{Pb}$	$\pm 2\text{SE}$	$^{206}\text{Pb}/^{238}\text{U}$ age	$\pm 2\text{SE}$	$^{207}\text{Pb}/^{235}\text{U}$ age	$\pm 2\text{SE}$	$^{207}\text{Pb-corr. Age}$	$\pm 2\text{SE}$
0.200	0.026	0.0189	0.0008	52.94	2.13	0.078	0.010	120.6	4.8	182	23	117.3	5.6
0.759	0.072	0.0248	0.0013	40.32	2.11	0.232	0.024	157.7	8.0	555	43	123.1	10.0
0.151	0.015	0.0195	0.0006	51.36	1.64	0.057	0.006	124.3	3.9	142	13	122.8	4.5
0.378	0.070	0.0200	0.0013	50.00	3.25	0.143	0.030	127.5	8.5	291	49	115.0	11.0
0.360	0.068	0.0209	0.0014	47.85	3.21	0.139	0.028	133.1	9.1	295	50	119.0	11.0
0.386	0.061	0.0203	0.0013	49.26	3.15	0.151	0.027	129.7	8.5	306	42	115.3	9.8
0.758	0.064	0.0244	0.0011	40.98	1.85	0.228	0.020	155.4	6.8	557	38	121.1	7.8
0.285	0.057	0.0198	0.0014	50.51	3.57	0.108	0.022	126.2	8.6	242	43	116.3	9.3
0.367	0.062	0.0215	0.0013	46.51	2.81	0.124	0.021	137.2	8.1	291	44	123.6	9.5
0.416	0.069	0.0219	0.0015	45.66	3.13	0.151	0.025	139.7	9.5	336	49	123.0	11.0
0.519	0.057	0.0223	0.0012	44.84	2.41	0.174	0.019	142.4	7.3	406	37	121.4	7.7
0.362	0.066	0.0209	0.0014	47.85	3.21	0.133	0.026	133.2	8.7	289	48	121.4	10.0
0.419	0.065	0.0218	0.0016	45.87	3.37	0.147	0.024	138.9	10.0	327	46	123.2	10.0
0.363	0.058	0.0213	0.0016	46.95	3.53	0.143	0.024	135.0	10.0	290	42	122.0	12.0
0.389	0.085	0.0210	0.0017	47.62	3.85	0.152	0.039	134.0	11.0	317	61	118.0	13.0
0.326	0.057	0.0194	0.0013	51.55	3.45	0.143	0.027	123.7	8.5	274	44	110.9	10.0
Sample CJ-12													
0.710	0.100	0.0236	0.0015	42.37	2.69	0.241	0.040	150.0	9.5	502	61	117.0	12.0
0.715	0.092	0.0241	0.0017	41.49	2.93	0.235	0.033	153.0	11.0	515	57	119.0	12.0
0.636	0.080	0.0238	0.0017	42.02	3.00	0.206	0.030	152.0	10.0	468	48	124.0	12.0
0.800	0.100	0.0250	0.0017	40.00	2.72	0.249	0.036	161.0	11.0	561	59	126.0	13.0
0.619	0.087	0.0245	0.0017	40.82	2.83	0.200	0.033	156.0	11.0	456	56	129.0	13.0
0.702	0.090	0.0239	0.0015	41.84	2.63	0.223	0.033	151.8	9.5	508	54	122.0	12.0
0.516	0.065	0.0237	0.0012	42.19	2.14	0.160	0.020	151.0	7.7	409	44	129.4	9.1
0.596	0.072	0.0243	0.0013	41.15	2.20	0.193	0.027	154.7	8.1	454	46	129.0	10.0
0.639	0.091	0.0232	0.0015	43.10	2.79	0.225	0.037	147.6	9.6	465	58	119.0	11.0
0.536	0.063	0.0230	0.0014	43.48	2.65	0.184	0.024	146.4	8.8	424	44	123.2	10.0
0.597	0.073	0.0240	0.0017	41.67	2.95	0.205	0.030	153.0	10.0	466	50	125.0	13.0
0.630	0.100	0.0234	0.0016	42.74	2.92	0.207	0.034	148.7	10.0	457	63	120.0	12.0
0.810	0.100	0.0248	0.0019	40.32	3.09	0.255	0.034	157.0	12.0	566	58	120.0	14.0
0.594	0.081	0.0238	0.0013	42.02	2.30	0.192	0.027	151.5	8.0	439	51	126.2	9.9
0.677	0.087	0.0260	0.0017	38.46	2.51	0.204	0.030	165.0	11.0	485	55	137.0	13.0
0.730	0.100	0.0242	0.0017	41.32	2.90	0.240	0.038	154.0	10.0	512	62	120.0	13.0
0.660	0.110	0.0238	0.0016	42.02	2.82	0.207	0.039	152.7	10.0	462	69	125.0	12.0
0.693	0.090	0.0241	0.0016	41.49	2.75	0.222	0.032	153.4	9.9	493	56	124.0	12.0
0.710	0.120	0.0271	0.0018	36.90	2.45	0.195	0.034	172.0	11.0	487	66	142.0	14.0
0.770	0.120	0.0248	0.0018	40.32	2.93	0.238	0.038	158.0	11.0	529	67	122.0	14.0
0.830	0.110	0.0255	0.0017	39.22	2.61	0.242	0.033	162.0	11.0	566	60	124.0	13.0
0.710	0.110	0.0252	0.0018	39.68	2.83	0.230	0.038	160.0	11.0	502	63	128.0	14.0
0.642	0.089	0.0255	0.0015	39.22	2.31	0.192	0.028	162.0	9.2	471	56	134.0	11.0
0.770	0.110	0.0235	0.0020	42.55	3.62	0.260	0.047	150.0	12.0	532	61	114.0	14.0
0.680	0.094	0.0231	0.0015	43.29	2.81	0.252	0.040	146.8	9.3	483	57	115.0	12.0
0.710	0.220	0.0245	0.0031	40.82	5.16	0.246	0.093	156.0	19.0	480	130	124.0	25.0
0.680	0.110	0.0241	0.0016	41.49	2.75	0.228	0.040	153.6	10.0	471	64	125.0	14.0
0.850	0.110	0.0262	0.0019	38.17	2.77	0.271	0.040	167.0	12.0	576	60	128.0	14.0
0.546	0.070	0.0240	0.0014	41.67	2.43	0.183	0.025	153.0	9.0	428	48	131.0	11.0
0.584	0.088	0.0236	0.0017	42.37	3.05	0.193	0.033	150.0	10.0	423	58	125.0	12.0
0.900	0.130	0.0260	0.0016	38.46	2.37	0.250	0.034	165.5	9.8	593	64	124.0	13.0
0.810	0.120	0.0264	0.0020	37.88	2.87	0.246	0.040	167.0	13.0	550	70	130.0	16.0
0.690	0.110	0.0245	0.0016	40.82	2.67	0.230	0.039	155.9	9.9	484	68	124.0	13.0
0.508	0.077	0.0238	0.0014	42.02	2.47	0.169	0.030	151.6	8.8	388	53	132.0	11.0
0.800	0.120	0.0254	0.0019	39.37	2.95	0.245	0.039	162.0	12.0	552	66	124.0	15.0
0.528	0.075	0.0246	0.0016	40.65	2.64	0.165	0.025	156.3	9.8	411	52	134.0	11.0

Table S2 (continued): Summary of laser ablation ICP-MS U–Pb titanite dating results.

Isotope ratios								Ages (Ma)					
$^{207}\text{Pb}/^{235}\text{U}$	$\pm 2\text{SE}$	$^{206}\text{Pb}/^{238}\text{U}$	$\pm 2\text{SE}$	$^{238}\text{U}/^{206}\text{Pb}$	$\pm 2\text{SE}$	$^{207}\text{Pb}/^{206}\text{Pb}$	$\pm 2\text{SE}$	$^{206}\text{Pb}/^{238}\text{U}$ age	$\pm 2\text{SE}$	$^{207}\text{Pb}/^{235}\text{U}$ age	$\pm 2\text{SE}$	$^{207}\text{Pb-corr. Age}$	$\pm 2\text{SE}$
0.710	0.130	0.0244	0.0025	40.98	4.20	0.231	0.050	155.0	16.0	513	83	123.0	18.0
Sample Czi-1-12													
1.050	0.120	0.0272	0.0015	36.76	2.03	0.299	0.039	172.9	9.1	681	59	124.0	13.0
0.471	0.049	0.0220	0.0011	45.45	2.27	0.157	0.017	140.4	7.0	386	34	122.1	7.7
1.070	0.190	0.0258	0.0028	38.76	4.21	0.313	0.062	164.0	18.0	704	92	113.0	21.0
1.060	0.110	0.0277	0.0014	36.10	1.82	0.283	0.032	175.9	8.5	694	56	125.0	11.0
0.726	0.052	0.0234	0.0009	42.72	1.64	0.235	0.021	149.1	5.7	541	31	117.0	7.5
0.860	0.170	0.0243	0.0020	41.15	3.39	0.251	0.046	155.0	13.0	585	88	115.0	16.0
1.010	0.120	0.0260	0.0016	38.46	2.37	0.304	0.039	165.4	10.0	675	62	116.0	13.0
0.463	0.067	0.0215	0.0011	46.51	2.38	0.157	0.024	137.3	7.0	370	46	118.7	8.3
0.820	0.130	0.0238	0.0016	42.02	2.82	0.256	0.044	151.6	10.0	575	72	113.0	13.0
1.007	0.095	0.0264	0.0013	37.88	1.87	0.288	0.030	167.9	8.0	683	48	121.0	11.0
1.350	0.160	0.0275	0.0022	36.36	2.91	0.381	0.055	175.0	14.0	848	65	110.0	19.0
1.590	0.140	0.0314	0.0018	31.85	1.83	0.405	0.047	199.0	11.0	930	57	120.0	16.0
1.040	0.130	0.0271	0.0016	36.90	2.18	0.298	0.038	172.0	9.9	683	65	121.0	11.0
0.783	0.077	0.0244	0.0012	40.98	2.02	0.243	0.025	155.2	7.8	561	45	119.6	8.8
0.417	0.032	0.0208	0.0007	48.03	1.61	0.147	0.012	132.8	4.4	347	23	116.9	4.8
0.855	0.095	0.0266	0.0017	37.59	2.40	0.255	0.033	169.0	11.0	597	55	129.0	13.0
0.930	0.130	0.0266	0.0023	37.59	3.25	0.267	0.044	169.0	14.0	647	67	126.0	17.0
0.620	0.063	0.0241	0.0012	41.49	2.07	0.203	0.023	153.1	7.4	470	38	126.1	9.0
0.658	0.051	0.0242	0.0009	41.41	1.53	0.200	0.017	153.8	5.6	500	31	125.2	7.0
1.870	0.340	0.0368	0.0036	27.17	2.66	0.381	0.077	233.0	23.0	1010	120	139.0	33.0
0.857	0.085	0.0257	0.0011	38.91	1.67	0.246	0.026	163.6	7.0	600	46	125.2	8.7
1.070	0.150	0.0269	0.0017	37.17	2.35	0.316	0.051	171.0	11.0	692	73	120.0	15.0
0.589	0.073	0.0245	0.0014	40.82	2.33	0.178	0.024	155.7	8.6	473	53	129.7	9.7
0.761	0.084	0.0240	0.0014	41.67	2.43	0.243	0.027	153.0	8.9	551	49	117.2	9.6
0.980	0.110	0.0272	0.0016	36.76	2.16	0.278	0.036	172.6	9.8	647	59	127.0	12.0
1.040	0.100	0.0275	0.0016	36.36	2.12	0.298	0.036	175.0	10.0	692	50	127.0	12.0
0.707	0.085	0.0238	0.0014	42.02	2.47	0.223	0.030	151.5	8.9	525	54	120.0	11.0
0.762	0.079	0.0235	0.0015	42.55	2.72	0.251	0.028	149.4	9.2	553	47	114.0	10.0
1.460	0.160	0.0309	0.0020	32.36	2.09	0.350	0.036	196.0	12.0	858	71	123.0	12.0
0.619	0.063	0.0228	0.0010	43.80	1.92	0.209	0.025	145.5	6.4	470	40	118.6	8.4
0.742	0.086	0.0260	0.0015	38.46	2.22	0.232	0.037	165.1	9.3	545	52	132.0	13.0
0.946	0.096	0.0271	0.0014	36.90	1.91	0.273	0.032	172.3	8.9	656	54	126.0	12.0
0.984	0.094	0.0255	0.0013	39.22	2.00	0.310	0.038	162.1	8.1	664	49	115.0	11.0
0.880	0.110	0.0250	0.0019	40.00	3.04	0.260	0.035	159.0	12.0	612	59	118.0	13.0
1.140	0.110	0.0287	0.0017	34.84	2.06	0.324	0.041	182.0	11.0	751	55	127.0	15.0
0.564	0.048	0.0226	0.0008	44.23	1.58	0.191	0.019	144.1	5.1	446	31	118.5	6.7
0.712	0.079	0.0246	0.0012	40.65	1.98	0.220	0.026	156.7	7.3	529	48	123.8	9.1
0.738	0.065	0.0237	0.0012	42.19	2.14	0.236	0.023	151.1	7.2	546	40	117.0	8.4
Sample CBH1-12													
0.688	0.068	0.0234	0.0011	42.74	2.01	0.227	0.025	148.7	6.6	500	41	119.3	8.3
1.137	0.086	0.0292	0.0013	34.25	1.52	0.303	0.027	185.4	8.2	742	43	131.0	10.0
0.715	0.072	0.0240	0.0012	41.67	2.08	0.226	0.024	152.9	7.8	522	44	119.2	8.9
0.128	0.025	0.0182	0.0007	54.91	2.17	0.049	0.010	116.3	4.5	115	21	115.9	5.1
0.265	0.042	0.0202	0.0010	49.58	2.34	0.099	0.016	128.6	6.0	231	33	120.2	6.8
0.830	0.098	0.0248	0.0014	40.32	2.28	0.262	0.034	157.7	8.9	583	55	119.0	11.0
0.822	0.057	0.0249	0.0009	40.16	1.39	0.244	0.019	158.5	5.4	594	32	120.7	6.4
0.566	0.076	0.0212	0.0014	47.17	3.11	0.198	0.029	135.4	8.6	431	51	110.0	10.0
1.317	0.093	0.0302	0.0013	33.11	1.43	0.337	0.029	191.7	8.4	837	41	126.0	11.0
0.676	0.076	0.0236	0.0012	42.37	2.15	0.228	0.030	150.1	7.5	510	48	118.8	9.7
0.561	0.074	0.0218	0.0013	45.87	2.74	0.182	0.027	139.2	8.1	428	47	115.4	9.9
0.803	0.082	0.0258	0.0013	38.76	1.95	0.250	0.030	163.8	7.9	572	50	126.0	10.0

Table S2 (continued): Summary of laser ablation ICP-MS U–Pb titanite dating results.

Isotope ratios							Ages (Ma)						
$^{207}\text{Pb}/^{235}\text{U}$	$\pm 2\text{SE}$	$^{206}\text{Pb}/^{238}\text{U}$	$\pm 2\text{SE}$	$^{238}\text{U}/^{206}\text{Pb}$	$\pm 2\text{SE}$	$^{207}\text{Pb}/^{206}\text{Pb}$	$\pm 2\text{SE}$	$^{206}\text{Pb}/^{238}\text{U}$ age	$\pm 2\text{SE}$	$^{207}\text{Pb}/^{235}\text{U}$ age	$\pm 2\text{SE}$	^{207}Pb -corr. Age	$\pm 2\text{SE}$
1.020	0.110	0.0270	0.0015	37.04	2.06	0.285	0.032	171.8	9.3	685	57	124.0	12.0
3.270	0.240	0.0482	0.0023	20.75	0.99	0.499	0.041	303.0	14.0	1440	60	140.0	19.0
0.555	0.046	0.0219	0.0008	45.60	1.66	0.186	0.017	139.8	5.0	434	30	116.3	5.7
0.576	0.077	0.0229	0.0013	43.67	2.48	0.204	0.029	145.7	8.1	433	50	120.2	8.8
0.646	0.068	0.0226	0.0011	44.25	2.15	0.231	0.030	143.8	7.0	488	43	115.3	9.1
0.127	0.019	0.0191	0.0006	52.25	1.56	0.049	0.007	122.2	3.6	117	16	121.7	4.0
4.250	0.230	0.0560	0.0023	17.86	0.73	0.559	0.036	351.0	14.0	1664	46	131.0	20.0
0.599	0.066	0.0216	0.0010	46.30	2.14	0.212	0.025	137.7	6.4	448	42	112.3	7.6
0.215	0.029	0.0192	0.0008	52.16	2.18	0.084	0.012	122.3	5.0	188	24	117.3	5.5
1.370	0.120	0.0291	0.0014	34.36	1.65	0.353	0.037	184.6	9.0	852	53	117.0	12.0
0.468	0.064	0.0216	0.0012	46.30	2.57	0.174	0.026	137.5	7.3	371	46	117.1	8.5
0.528	0.061	0.0226	0.0012	44.25	2.35	0.190	0.026	144.2	7.3	404	42	122.5	9.1
0.817	0.061	0.0236	0.0009	42.30	1.61	0.262	0.022	150.5	5.7	590	35	113.1	7.2
Sample CR6-11													
0.416	0.047	0.0218	0.0010	45.79	2.10	0.145	0.018	139.1	6.4	335	34	123.3	7.1
0.401	0.067	0.0214	0.0013	46.73	2.84	0.156	0.032	136.6	8.0	312	48	120.4	9.8
0.577	0.068	0.0224	0.0011	44.64	2.19	0.204	0.026	142.8	7.0	436	45	117.0	9.1
0.482	0.069	0.0218	0.0013	45.87	2.74	0.165	0.025	138.7	8.1	369	48	118.1	9.2
0.377	0.046	0.0214	0.0009	46.82	2.06	0.132	0.017	136.1	6.0	315	35	120.7	6.7
0.495	0.054	0.0215	0.0009	46.45	2.01	0.177	0.021	137.9	6.0	391	37	117.0	7.4
0.366	0.045	0.0214	0.0010	46.82	2.19	0.134	0.018	136.1	6.3	299	34	123.0	7.3
0.249	0.031	0.0192	0.0009	52.16	2.34	0.103	0.013	122.3	5.4	223	26	114.6	6.1
0.396	0.064	0.0219	0.0012	45.66	2.50	0.141	0.026	139.8	7.6	314	47	124.0	8.9
0.329	0.053	0.0201	0.0010	49.75	2.48	0.138	0.024	128.3	6.6	262	40	118.0	8.5
0.345	0.051	0.0207	0.0010	48.31	2.33	0.127	0.020	132.2	6.5	271	37	120.4	7.4
0.298	0.045	0.0211	0.0011	47.39	2.47	0.112	0.019	134.5	7.1	244	35	125.1	8.1
0.351	0.047	0.0212	0.0010	47.19	2.16	0.126	0.018	135.0	6.1	282	34	123.9	7.6
0.364	0.061	0.0206	0.0013	48.54	3.06	0.147	0.026	131.1	7.9	292	46	116.9	9.1
0.674	0.065	0.0225	0.0010	44.42	1.87	0.225	0.022	143.4	6.0	498	39	112.6	6.9
0.442	0.073	0.0204	0.0014	49.02	3.36	0.165	0.032	130.0	8.7	339	50	112.0	10.0
0.400	0.057	0.0204	0.0011	49.02	2.64	0.155	0.025	129.8	7.1	318	41	112.8	8.1